25 PRODUCTION PHASE OPTICAL TESTS

25.1 INTRODUCTION

25.1.1 General. Intrinsic in the design of most optical systems is the calculation of the Seidel aberrations. In this section we will outline procedures for measuring these aberrations experimentally during either the production or the evaluation phase. In this connection it should be noted that over the years different laboratories have developed their own techniques for making these measurements. Frequently the difference between techniques is not so much a matter of difference in basic principle, as it is in the equipment that a particular laboratory happens to have on hand. While there are, then, many, many different ways to make each measurement, we will limit ourselves to one example of each. The interested reader may consult the references for additional information.

25.1.2 Theory vs practice. Before leaving this introduction to the measurement of Seidel aberrations, a few words of caution are in order. Aberrations may be completely isolated only in theory. The actual image embodies, simultaneously, all aberrations pertaining to it. This, of necessity, complicates the measurement, and particularly complicates the detailed checking of the theoretical predictions as to the values of the individual aberrations. It should be pointed out also that the accuracy with which the aberrations need to be measured is a function of the importance of the particular aberration to the job at hand. The experiments to be described generally assume a white light source. Chromatic effects are determined by use of the appropriate filters.

25.2 FOCAL LENGTH

25.2.1 Importance of focal length. Certainly one of the fundamental constants of any optical system that is of prime importance in the evaluation of the significance of all Seidel aberrations is focal length. Not only is the value of the focal length of importance, but also a precise statement of the point from which the focal length is to be measured is mandatory. Some years ago an aerial camera lens was designed and simultaneously the camera body was fabricated, presumably for the same focal length systems. When the lens was installed in the body, a photographic check showed hardly any semblance of an image. To say that it was "out of focus" was charitable. The error was tracked down ultimately to the fact that focal length meant measurement from the secondary principal point to the lens designer and meant from the rear surface to the machinist. Through human error, both lens and body were allowed to be fabricated on this erroneous basis. Since the secondary principal point lay several inches inside the lens, the horribly blurred image was not surprising. Recently a similar situation developed in a missile-tracking system where the optical designer measured the focal point with respect to the front surface and the machinists assumed that it was measured from the rear surface (the optics involved a thick mirror). Since the system was quite fast with short focal length, the one inch central thickness of the thick mirror played havoc with the performance of the system when finally assembled.

25.2.2 Measurement of focal length. While there are many methods for measuring the focal length of an optical system [1] [2] [3] [4], one of the most accurate for lenses of medium focal length employs the nodal slide. A photograph of one in use at the National Bureau of Standards is shown in Figure 25.1. The essential part of the nodal slide is the provision for moving the lens system longitudinally with respect to a vertical axis of rotation. This vertical axis is mounted so that it may be positioned longitudinally with respect to a collimator of appropriate size. Usually the object for the collimator is a very small point source set at the focal point of the collimator.

25.2.3 Test setup. The equipment is set up as shown schematically in Figure 25.2. In use the magnifier or microscope is set up approximately at the focal point. The lens under test is then moved backward and forward along the nodal slide until rotation of the nodal slide through a small angle, B, produces no sidewise shift in the image. The focal length is then the distance between the axis of rotation of the nodal slide and the appropriate focal point of the magnifier or microscope. There are many variations on this technique, some employing auto collimation, some focusing the image on a card, etc. Negative optics may also be tested in this manner by the addition of a positive lens of known characteristics. Knowing the position of the secondary nodal point (coincides with the principal point if the index of refraction of image space is air), the focal length may be specified with respect to the vertex of the rear surface (this distance is known as the "back focal length") or to any other convenient part of the lens.

(1) Cheshire, Trans. Optical for (London) 22, 29 (1920-1921).
(2) Kurtz, Jour. Opt. Sci. of Am. and Rev. of Sci. Instr. 7,103 (1923).
(3) Searle, Experimental Optics, Exp. 37, 185 Cambridge Univ. Press (1925).
(4) Wagner, Experimental Optics, Exp. 67, 136, Wiley (1929).

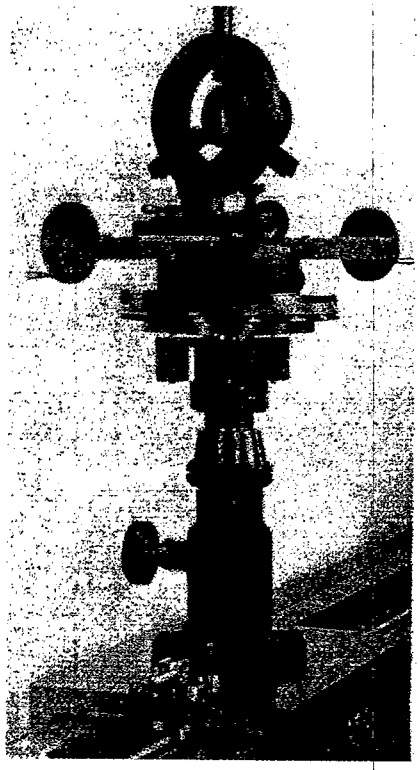

Figure 25. 1- Nodal slide developed at the U. S. National Bureau of Standards.

L_c = collimating system

L_x = system under test

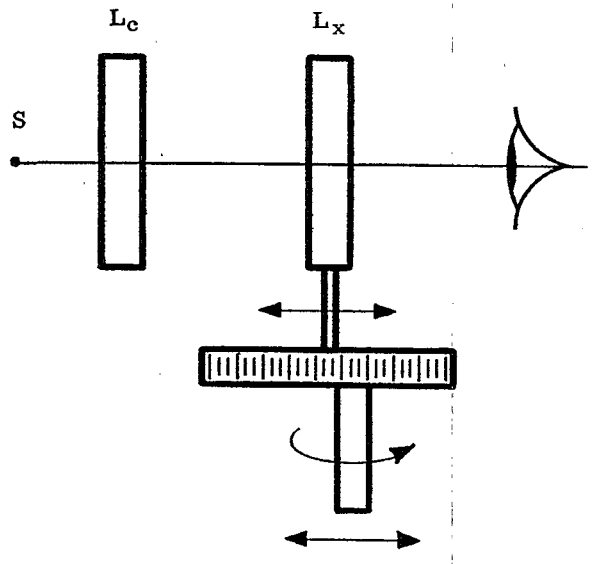

Figure 25. 2- Measurement of focal length by use of visual nodal slide.

25.3 LONGITUDINAL SPHERICAL ABERRATION

25.3.1 On-axis performance. Of considerable importance in almost all optical systems is the on-axis performance. Since the principal use of many visual optical systems is tracking in one form or another, systems are ultimately pointed directly at the target. The nature of the image on-axis is thus important. A factor also of much significance is the degree to which the system may be "opened up" and still maintain a good image. This latter requirement involves spherical aberration.

25.3.2 Hartmann test. While there are many techniques for doing this [5] [6], the simplest is perhaps the Hartmann test [7] [8] [9]. It may be done either photographically or visually and can be made reasonably sensitive. It is probably not as accurate as a newer method developed by Washer, but is chosen here for its directness and simplicity.

25.3.3 Test procedure. Blocking off all but holes 1 and 8 in the Hartman Disk shown in Figure 25.3 will give the marginal focus. Holes 2 and 7 should be located at the zonal positions, and their intersection will give the zonal focus. The paraxial focus may be determined with holes 4 and 5, or by direct inspection of the lens stopped down to a very small circular aperture. From the data just obtained the longitudinal spherical aberration may be determined. Filters may be used to get the aberration for different colors if so desired.

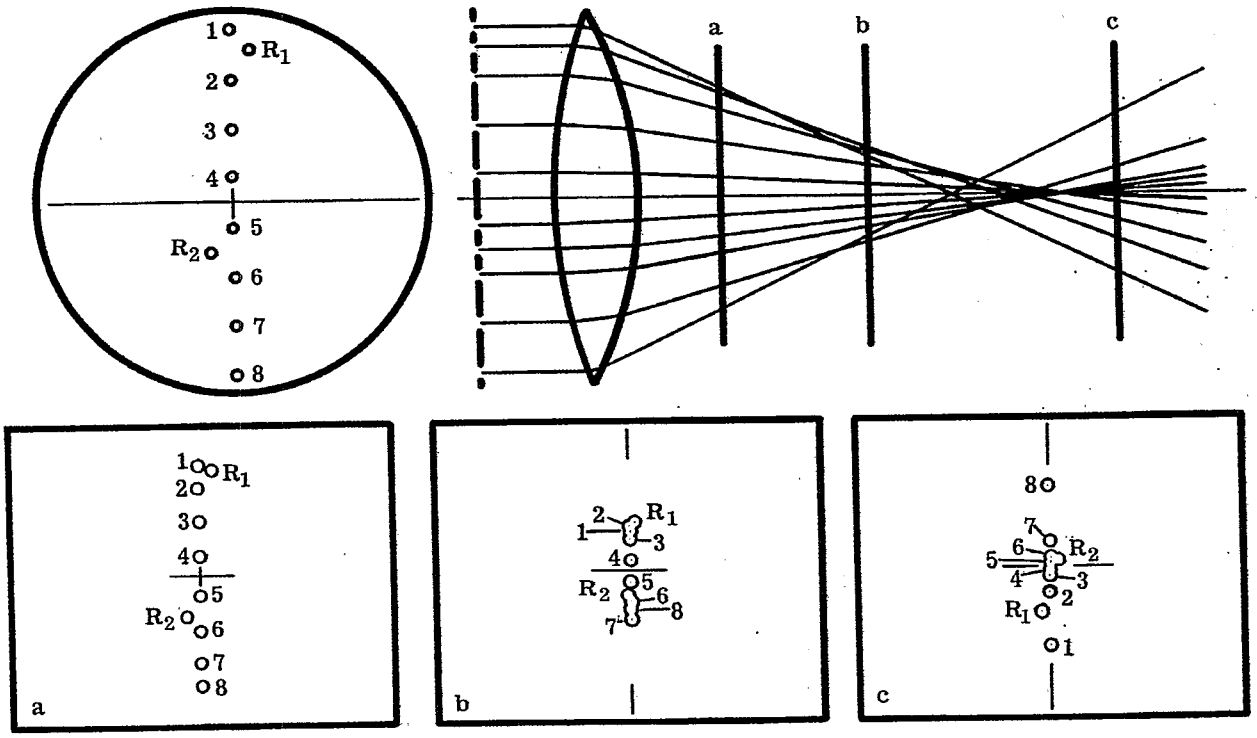

Figure 25.3-Measurement of spherical aberration by the Hartman Test.

(After Strong's, Concepts of Classical Optics, W.H. Freeman and Co. 1958)

(5) Washer, Jour. of Res. of Nat'l Bureau of St'nds 61, No. 1, 31, (July 1958).
(6) Monk, Light-Principles and Experiments 349, McGraw-Hill (1937).
(7) Strong, Concepts of Classical Optics, 354 Freeman (1958).
(8) Hartmann, Zeit. f. Inst. XX IV, 1 (1904); and subsequent papers in 1904.
(9) Bureau of Standards Scientific Papers No. 311 and 494.

25.4 COMA

25.4.1 Asymmetrical flare. Asymmetrical flare produced by coma is one of the most important aberrations to eliminate. The reason for this is that most of the other aberrations produce an image degradation that is more or less symmetrical with respect to the principal ray. For example this means that even though astigmatism may be present, the system may be pointed with a high degree of accuracy by centering the point of greatest density of the image on the cross hairs, etc. When the image is degraded asymmetrically, this same procedure can produce a pointing, or boresight, error.

25.4.2 Collimator check for coma. Coma, being an off-axis aberration, is somewhat difficult to separate from astigmatism. Usually in testing optical systems the optician will simply use a collimator to illuminate his lens at successive angles off axis. The focal plane image is then studied, and, if the flare is more than that allowed in the specifications, the system is reworked.

25.4.3 Hartmann disk. Coma may be demonstrated to a fairly successful degree by use of the Hartmann disk placed before the lens with the lens illuminated by off-axis parallel light and image space then studied, as indicated in the measurement of spherical aberration. Another simple method for measurement of coma using the Hartmann method is described in Hardy and Perrin [10], and refers to a method described previously in the National Bureau of Standards Scientific Papers No's. 311 and 494.

25.5 ASTIGMATISM AND CURVATURE OF FIELD

25.5.1 Measurement of astigmatism. Astigmatism may be measured accurately by a series of Foucault Tests with the knife edges at right angles in the basic manner described in the section devoted to the Foucault test. It may also be measured quite simply by the arrangement illustrated in Figure 25.4. In practice, the lens under test, L_x, is rotated and the traveling microscope, M, is adjusted until the image of the reticle, R, is found. The microscope is then adjusted; first until the vertical lines are in best focus; then until the horizontal lines are in best focus. L_x is then rotated to successive angles up to the maximum field angle, and the positions of best focus as just described measured at each angle. A plot of the positions of best focus for the vertical lines will give the sagittal (secondary) focal surface, and the corresponding plot of the positions of best focus for the horizontal lines will give the tangential (meridional or primary) focal surface. The reason why the tangential plane images the horizontal lines best is shown clearly in Jenkins and White [11]. The microscope must of course be movable laterally as well as longitudinally to examine the astigmatism at various points on the focal plane. If in addition to making determinations of the position of best focus of the horizontal and vertical lines, one also notes the position of best overall focus of the central point in the grid system, the curvature of field may be determined.

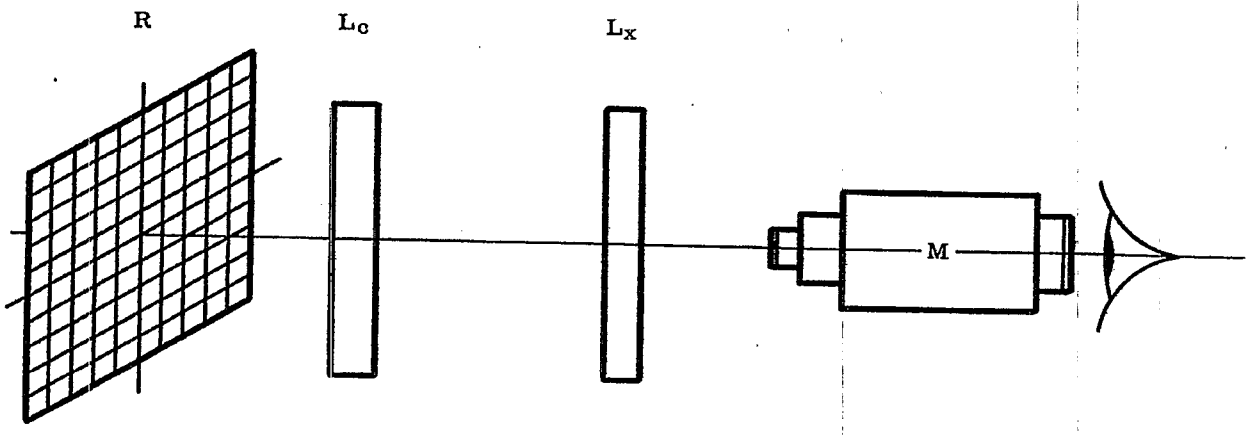

Figure 25.4- Measurement of astigmatism with a grid reticle.

(10) Hardy and Perrin, The Principles of Optics, 382, McGraw-Hill, (1932).
(11) Jenkins and White, Fundamentals of Optics, (2nd edition), 139, McGraw-Hill, (1950).

25.5.2 Determination of curvature of field. Generally, curvature of field may be determined with respect to the flat focal plane of a camera by placing a flat glass plate with a grease pencil mark across a diameter in the position occupied by the film. The grease pencil mark is towards the camera lens. One then notes the position of the traveling microscope when focused on the grease pencil mark. The camera being set up similar to that in Figure 25.4, the microscope is then focused on a star image (or central point of the reticle). The difference between the two readings is a measure of the curvature of field. Curvature of field measurements are very important in visual systems as the curvature of field of the object must match that of the eyepiece or else considerable image degradation ensue.

25.5.3 Consistency of test procedure. One should note clearly in all of these testing methods that if a system is to be used visually, then ideally it should be tested visually. Photographic testing does have its advantages, however, as it furnishes a record.

25.6 DISTORTION

25.6.1 Importance of distortion study. In optical systems designed essentially for visual observation and study of objects on-axis, the aberration known as distortion is really not too important. There are many systems, however, where, while the target may be centered in the eyepiece, measurements must be made over the entire field of view. An example of such a system is a rangefinder.

25.6.2 A rapid check for distortion: Distortion may be measured photographically very simply by replacing the microscope in Figure 25.4 by a good quality camera, known to be well corrected over the field of the optical system under test. The grid reticle is then photographed and the distortion, whether pin cushion, barrel, or irregular, is immediately obvious when D is set = 0.

25.6.3 An accurate distortion measurement for small optical systems. An excellent method of making this measurement for small optical systems with the basic nodal slide has been outlined by Washer, Tayman, and Darling [12]. The procedure is as follows:

(a) The optical system under test is placed on the nodal slide shown in Figure 25.2.

(b) A measuring microscope is adjusted with respect to the lens until a focus is found.

(c) The lens system is then moved in the usual way along the nodal slide until small rotations (the microscope having been kept in focus by longitudinal movement) show no lateral movement of the image.

(d) Assuming that the focal length, f, is now measured or known, it is clear that if the microscope were moved off-axis yet remaining in this focal plane that the distance to the lens would now be f sec β.

(e) If now, instead of moving the microscope, the lens is rotated in the nodal slide by an angle β and moved longitudinally a distance (f sec β - f) or f (sec β - 1) toward the collimator, the microscope should again see the image clearly. Actually the image will probably not be on-axis and the microscope will have to be moved laterally a small distance to pick it up again.

(f) The reading of the micrometer measuring this lateral shift is noted as R.

(g) The lens is now rotated through an angle $-\beta$ and the microscope, when repositioned, gives a reading L.

(h) The distortion, D, at the angle β, is then given by the simple expression,

$$D_\beta = \frac{(R-L)}{2} \sec \beta \qquad (1)$$

25.7 AUXILIARY OPTICAL MEASUREMENTS

25.7.1 Introduction. In the fabrication and testing of optical instruments, it is frequently necessary to make measurements that are made considerably less frequently in regular machine shops. One of these measurements is the radius of curvature of spherical and aspherical surfaces: another is the measurement of the index refraction.

25.7.2 Radii of curvature.

25.7.2.1 The radius of curvature of an optical surface whose diameter is on the order of 1 - 3" may be done very conveniently with a spherometer [13]. This device takes many forms--one of which is shown in Figure 11.9.

(12) Washer, Tayman, and Darling, Journal of Res. of N.B.S., 61, No. 6, 509 (1958).
(13) op. cit., (10), pg. 366.

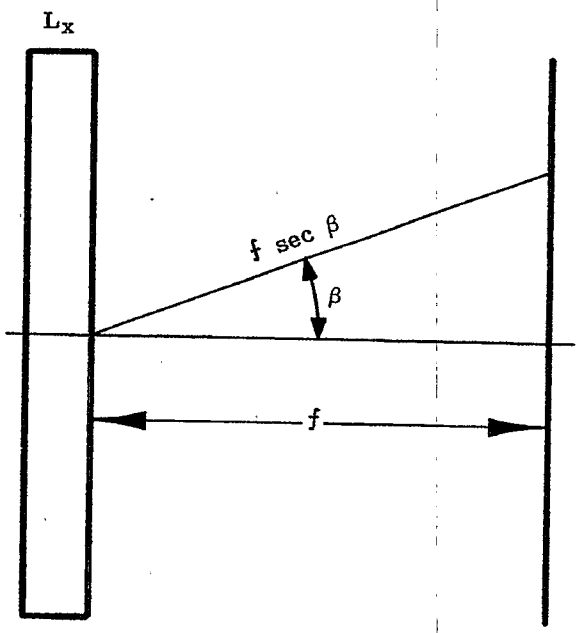

Figure 25.5- Basic diagram for measurement of distortion by nodal slide.

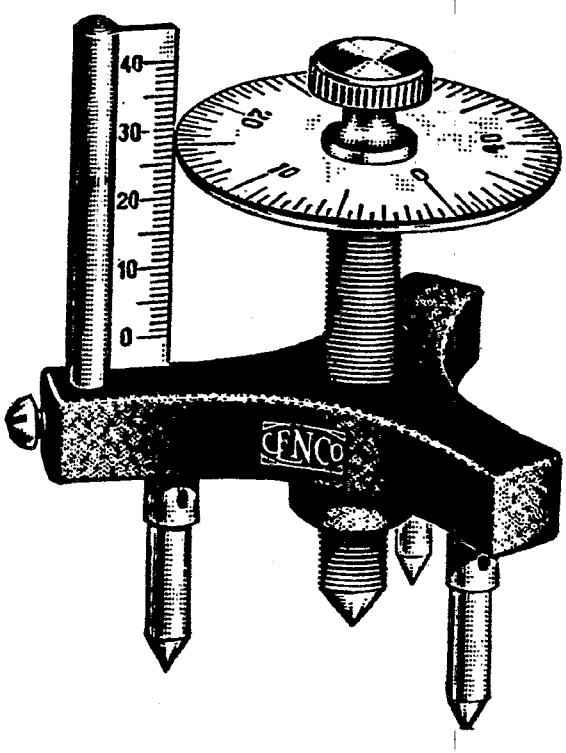

Figure 25.6- Elementary spherometer.

25.7.2.2 In use, the central spindle is screwed up and the three legs placed on the surface in question. The spindle is screwed down until it just touches the surface. The spherometer is then placed on a flat surface and the distance, S, the spindle must be advanced to meet the flat is noted. The procedure is reversed for a concave surface. The radius of curvature of the surface is then obtained from the following equation,

$$r = \frac{d^2}{6s} + \frac{s}{2} \qquad (2)$$

where d = the average distance between the legs.

25.7.2.3 For large surfaces the Foucault method described in paragraph 25.8.2 is used. For very small surfaces, less than about an inch across, a different method is employed. A provision is made for illuminating from the side, the cross hairs or reticle of a Gauss eyepiece, or equivalent, in a microscope or short focal length telescope (the choice depending upon the curvature of the sample to be tested). The microscope is focussed first on the surface of the sample, and the longitudinal position of the microscope recorded. The microscope is then racked back until there is no parallax between the illuminated cross hairs and the image from the surface. The cross hairs are then at the center of curvature. This position of the microscope is also recorded. The difference between the two positions is the radius of curvature. A telescope would be used in exactly the same way for greater radii of curvature. A similar technique can be used for positive surfaces.

25.7.3 Index of refraction.

25.7.3.1 Where it is possible to grind and polish a small sample of the material, the spectrometer furnishes a very fundamental method for measuring the index of refraction. The theory and method are outlined in Hardy and Perrin (14) and Sawyer (15). With a good spectrometer the values of the index so determined are good to ± .00003. A high precision spectrometer is shown in Figure 25.7.

25.7.3.2 For many samples it is not possible to get the sample in the form required for the spectrometer and for these the refractometer is frequently well suited. One of the many refractometers is the Pulfrich (16). This method, based on refraction at the critical angle, will give values correct to ± 2 parts in the fifth decimal place, and is shown schematically in Figure 25.8.

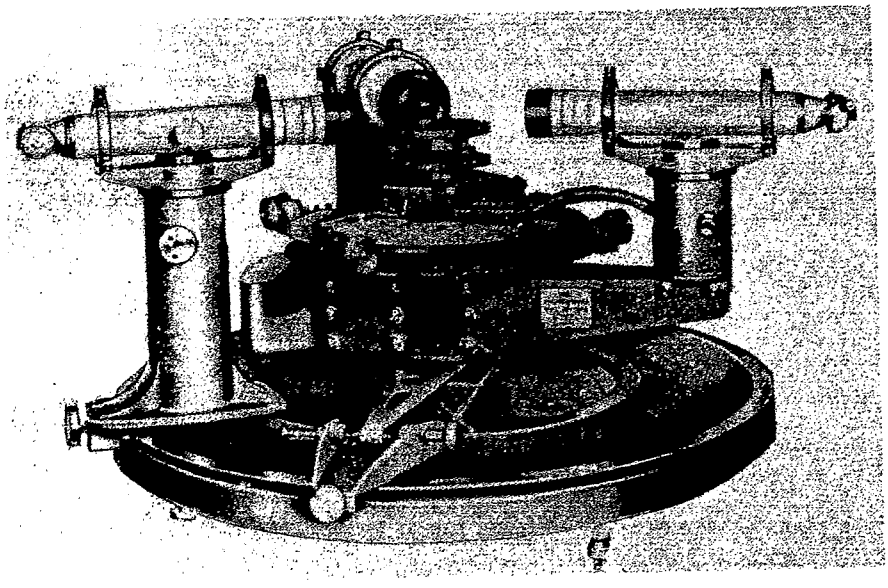

Figure 25.7 - The Guild-Watts precision spectrometer.

(14) op. cit., (10), 549
(15) Sawyer, Experimental Spectroscope, 55, Prentice Hall, (1944).
(16) op. cit., (10), 350.

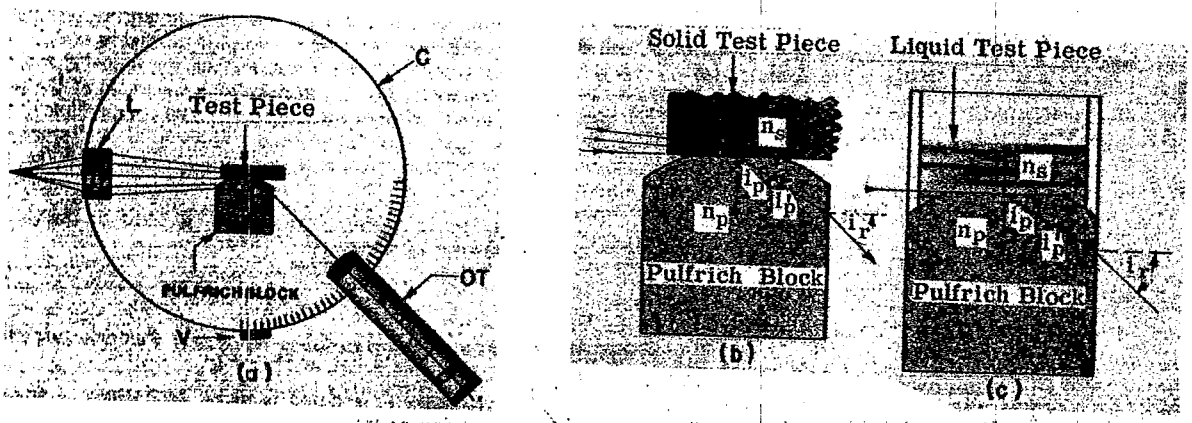

L = Converging lens
V = Vernier
C = Graduated Circle
OT = Observing Telescope

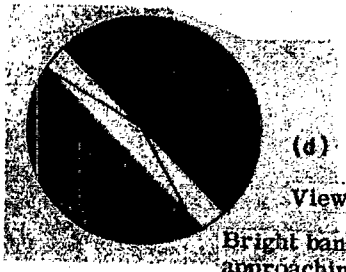

(d)

View through OT.

Bright band represents rays approaching at the critical angle.

The index of refraction of the sample is determined by

$$n_s = \sqrt{n_p^2 - \sin^2 i_r}$$

Figure 25.8 - Schematic of the Pulfrich refractometer.

25.8 OPTICAL DEVICES, TESTING SYSTEMS AND PROCEDURES

25.8.1 Interferometry principles.

25.8.1.1 The most common and simplest method for testing flatness of polished surfaces of glass or other transparent material utilizes interference fringes that are formed between the tested surface S_1 and an optically flat surface S_2 as illustrated in Figures 25.9 and 25.10. The preferred source of light is an unfiltered, tubular, Cooper-Hewitt lamp, L, which is provided with a diffusing reflector, R, and a diffusing glass plate, G. The advantage of the arrangement of Figure 25.9 is that it permits the interference fringes to be viewed at normal incidence. The positions of the light source and the eye may be interchanged. Figure 25.10 illustrates the most common arrangement where viewing at normal incidence is sacrificed to gain greater freedom as regards working space. The light emitted by the Cooper-Hewitt mercury lamp is preponderantly green. It can be rendered quite monochromatic at 5461 A, whenever desired, by means of readily available optical filters that can be held near the eye. The interference fringes are usually viewed in unfiltered light. Contrast in the fringes is improved by placing black felt or paper beneath the optical flat in the manner indicated.

25.8.1.2 It should be noted that the interferometer surfaces S_1 and S_2, Figures 25.9 and 25.10, are in close contact. Excess dust and other dirt must be removed in order to reduce the thickness d of the air-film between surfaces S_1 and S_2. Because the separation d of the surfaces S_1 and S_2 is small, the resulting interference fringes belong to a select class of fringes known as Fizeau or as Newton's fringes. The principles underlying these fringes have been discussed in paragraphs 16.12.1.2 and 16.13.1.5. These fringes are characterized by the following important properties and propositions.

(a) The interference fringes appear in good contrast when one focuses upon the air-film between the interferometer surfaces, S_1 and S_2, provided that the reflectances of these surfaces are approximately alike. It is often said that the fringes appear to be localized in the film.

(b) Because the separation, d, of the interferometer surfaces is small, the location laterally of the fringes between the surfaces does not depend markedly upon the angle of incidence, provided that one views the fringes approximately along the normal to the surfaces S_1 and S_2.

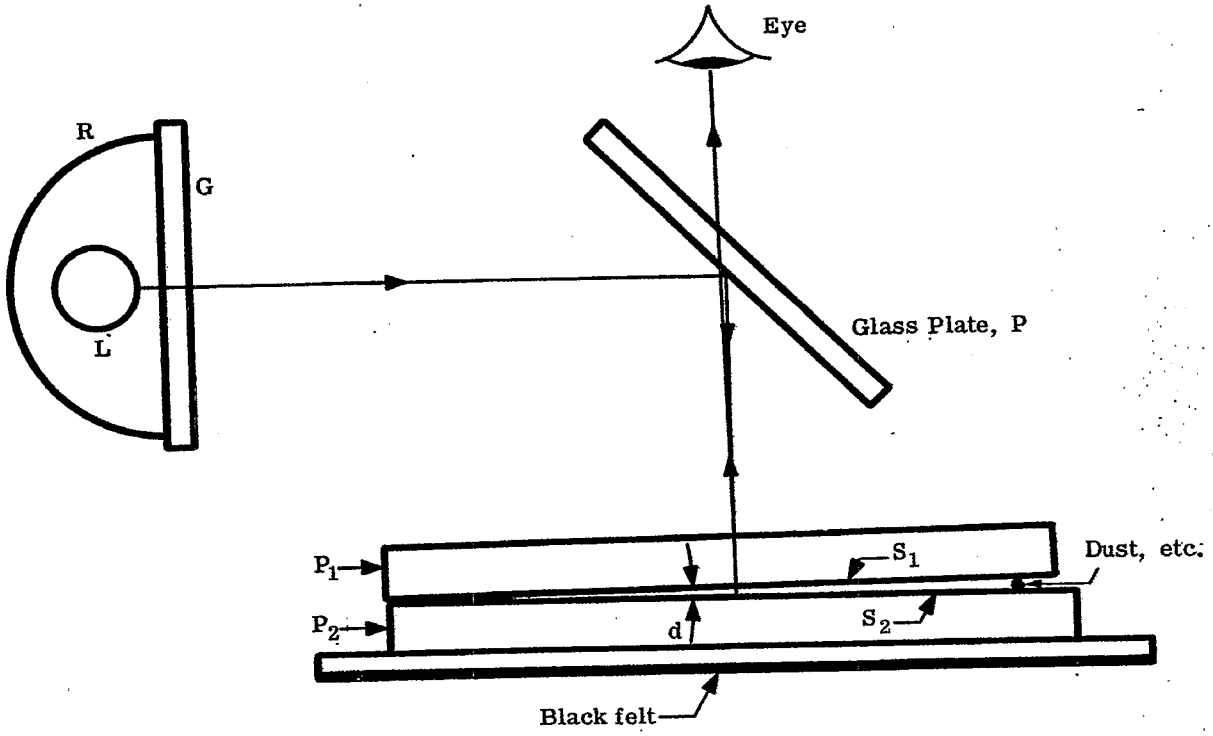

Figure 25.9 - Simple interferometer for viewing Fizeau fringes or Newton's fringes at normal incidence.

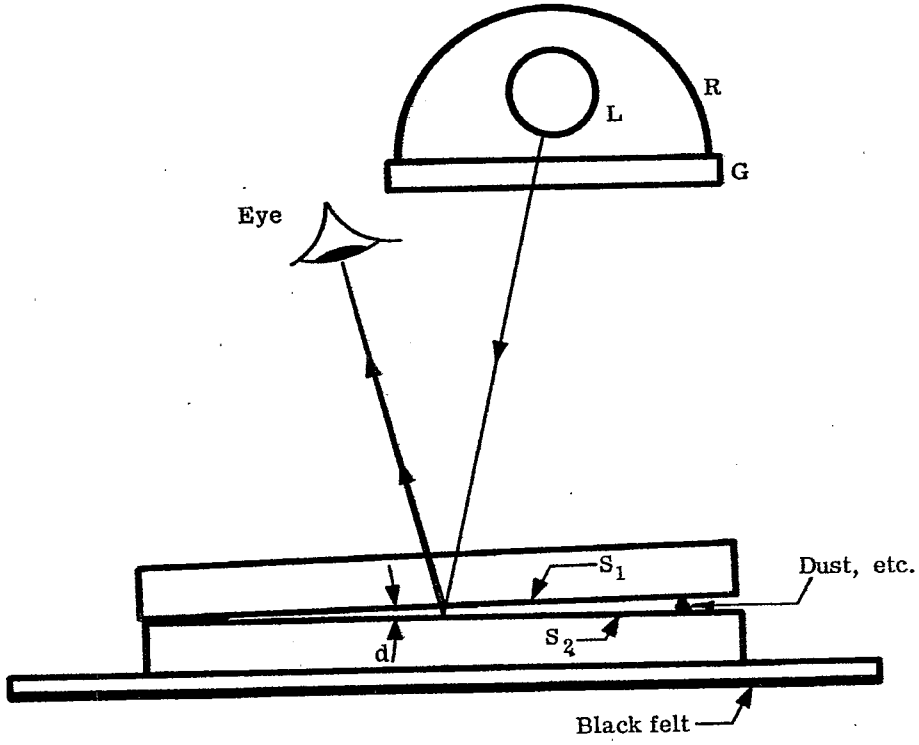

Figure 25.10- Most commonly used method for illuminating the interferometer. The fringes formed between surfaces S_1 and S_2 are observed at near - normal incidence.

(c) Each fringe marks the locus (lateral) of points for which the separation, d, is a particular constant. This constant is different for each fringe.

(d) When either surface is moved or distorted by the application of force or heat, each fringe moves in such a direction as to maintain the constant separation, d, associated with that fringe.

(e) Upon passing from one fringe to the next fringe of equal brightness or darkness, the separation, d, changes by one half wavelength.

(f) Upon passing from a bright fringe to the next dark fringe, the separation, d, changes by one fourth wavelength. It is assumed tacitly in (e) and (f) that the surfaces do not possess discontinuous jumps.

(g) When surfaces S_1 and S_2 are of nonabsorbing materials such as glass, dark fringes occur at separations, d, for which

$$d = \nu \frac{\lambda}{2} \; ; \; \nu = 0, 1, 2, 3, 4, \text{ etc.} \qquad (3)$$

and bright fringes occur at separations, d, for which

$$d = \mu \frac{\lambda}{4} \; ; \; \mu = 1, 3, 5, 7, \text{ etc.} \qquad (4)$$

wherein λ denotes wavelength.

Of these propositions and properties, (c) and (d) are of the greatest importance to the maker of optical flats. These two propositions or rules enable him to interpret the fringes for high and low areas on the surface under test. The optical worker recognizes fringes as contour lines on a contour map of his surface. Movement of the fringes upon application of pressure serves to distinguish the up-hill direction. Propositions (e) through (g) reveal the heights between contour lines. It is emphasized that propositions (e) and (f) are more general (and hence more often correct) than (g).

25.8.1.3 As one tests for flatness of a surface, the fringes become straighter as the surface becomes flatter. The effect of reducing the angle of the air-wedge between surfaces S_1 and S_2 by the removal or crushing of dust particles, is to widen the fringes and to increase their curvature except when S_1 is optically flat. Let, h denote the fringe width, i.e. the distance from one bright fringe to the next. For optical flats of high quality, the degree of flatness can be specified by requiring that any fringe shift from straightness shall not exceed a stated fraction of the fringe width, h, over a stated diameter or other dimension of the tested surface. As an example of the sensitivity of the method, a fringe shift h/5 corresponds to a change of separation, d, by the amount $\lambda/10$. Fringe shifts smaller than h/10 become difficult to detect and to measure in this type of interferometer.

25.8.1.4 In a second, and often preferred test for optical flats of high quality, the surfaces S_1 and S_2 are placed so closely in contact or are rendered so nearly parallel that a single fringe spreads over surface S_1. This broad fringe is examined for uniformity of color with an unfiltered source of light. It is customary to specify without further qualification that the surface shall be "polished to a uniform color".

25.8.1.5 The following procedure applies to that great class of test cases in which the departure of more than one fringe from flatness is tolerated. If the test surface is convex, only one area will contact the reference flat and this area will be surrounded by a number of alternately dark and bright Newton's fringes. The specification of flatness may be stated as the number of allowable Newton's fringes per inch, or other unit. If the test surface is concave, a ring-shaped area will contact the reference flat. The number of concentric fringes within this area can be counted and compared with the maximum tolerable number of Newton's fringes per inch or other unit. In practice, the surface S_1 is likely to display one or more convex or concave areas. Close examination of the fringes will distinguish between these convex and concave areas. If pressure is applied to a convex area in such a manner as to reduce the separation, d, between surfaces a given fringe about the area of closest contact must move outward from its center in order to maintain the locus of points for which d is a given constant.

25.8.1.6 No essential modification of the method of Figures 25.9 or 25.10 is needed for testing spherical surfaces. The reference flat, S_2, is replaced by a concave or convex reference surface whose radius is equal to the desired radius of the completed test surface. Suppose that surface S_1 has a smaller radius than surface S_2 as illustrated in Figure 25.11. Concentric Newton's fringes will appear around point O. The maximum allowed number of Newton's fringes per inch along the radial direction from O may be stated as the permissible departure of surfaces S_1 from the "test glass" having the surface of reference S_2. For surfaces, S_1, of high optical quality, the radius of surface S_1 will be made to match that of S_2. At the match point, it will

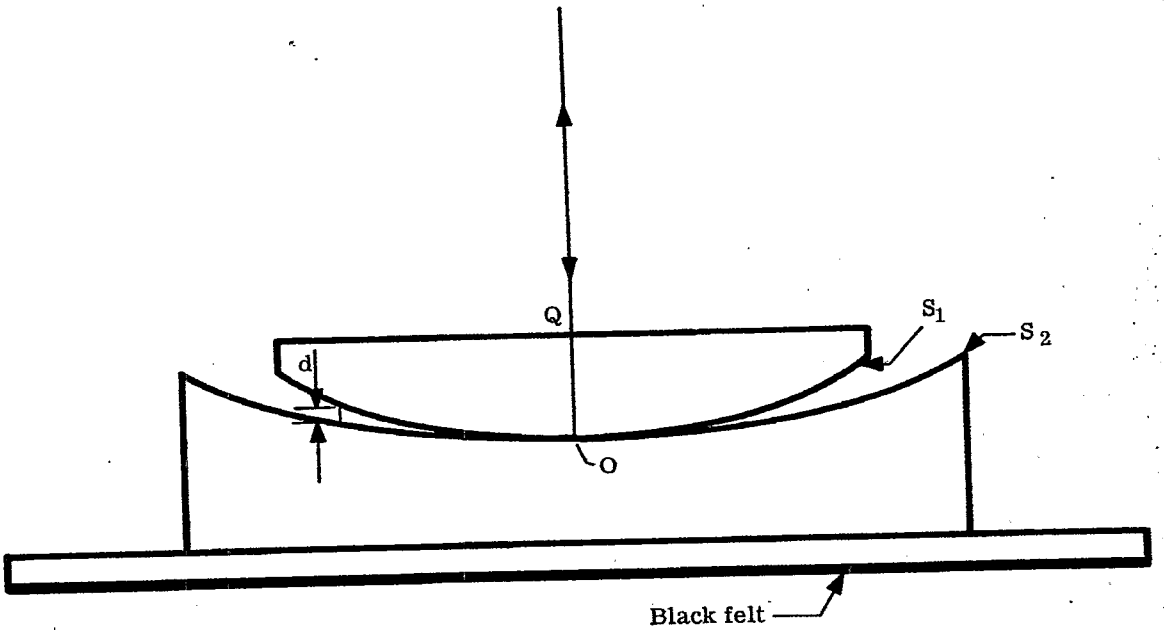

Figure 25.11- Arrangement of the interferometer surfaces S_1 and S_2 for obtaining Newton's fringes.

be possible, as in paragraph 25.8.1.4, to place surfaces S_1 and S_2 into sufficiently close contact so that a single fringe spreads over surface S_1. For work of highest quality, it is customary to specify that this single fringe shall be made uniform in color.

25.8.1.7 The method of the sagitta (see paragraphs 16.13.1.1 and 16.13.1.6) enables one to make a good estimate of the radius of surface S_1 when this radius departs only slightly from that of the test glass. Consequently, it is not always necessary to provide a test glass whose radius is equal to that of the completed surface S_1.

25.8.1.8 When elliptical fringes appear around point O, Figure 25.11, surface S_1 is not spherical. The minor and major axes of the elliptical fringes may be measured, and the ratio of the minor axis to the major axis computed. This ratio is a measure of the ellipticity of surface S_1 and is often utilized as a specification of the maximum tolerable ellipticity. When departures of many fringes from the test glass can be tolerated, another measure of ellipticity is to count the number of fringes along some convenient length in the direction of the major and minor axes of the elliptical fringes and to utilize the ratio of these fringe counts in specifying the tolerable ellipticity.

25.8.1.9 An extreme amount of irregularity in the shape of the fringes is an indication that the tested surface has been improperly polished or molded. "Orange peel" and other defects of polished surface produce irregularities in the observed pattern of fringes.

25.8.1.10 Contrast in the fringes deteriorates as the reflectances a_1 and a_2 of surfaces S_1 and S_2 become more unlike. The light beams reflected from these two surfaces can interfere to produce systems of fringes having zero intensity in the dark fringes (and hence displaying maximum contrast) only when the amplitudes, a_1 and a_2, of the two, coherent, interfering beams are alike. The distribution of intensity in the fringe system when a_1 and a_2 are unlike can be ascertained from paragraphs 16.1.1.3, 16.1.1.5, 16.8.1.1, 16.8.1.2, and 16.9.1.4 . In spite of reduced contrast in the fringes, the interferometers of Figures 25.9 and 25.10 are often applied to testing polished surfaces of metals. With metals and other opaque substances, surface S_2 of Figures 25.9 and 25.10 must be that of the opaque material.

25.8.1.11 The reflectance of the "test glass" can be increased by the deposition of a high reflecting coating or by increasing the refractive index of the test glass. In this way, contrast in the fringe system will be improved in testing high reflecting surfaces. Metallic surfaces and coatings produce phase changes on reflection

that differ from zero (as in the reflection from a glass-to-air interface) or that differ from $\lambda/2$ (as in the reflection from an air-to-glass interface). Consequently, Equations (3) and (4) require modification. However, the effect of the modified phase changes on reflection is only to shift the location of the fringes. As a result, the interpretation of sections 25.8.1.3 to 25.8.1.9 remains unchanged when applied to coated or metallic surfaces. For testing surfaces of high quality, any coating applied to the test glass must be extremely uniform in thickness and composition because phase changes on reflection can vary appreciably with thickness and composition of the coating.

25.8.1.12 As the reflectance of surfaces S_1 and S_2 is increased from that of polished glass, the nature of the interference fringes formed by the interferometers of Figures 25.9 and 25.10 alters gradually until, finally, these fringes are classified as multiple beam interference fringes. Inter-reflections between surfaces S_1 and S_2 serve to sharpen the fringes formed by the reflected or the transmitted light beams in the manner discussed in paragraph 16.17. With suitable changes in the technique of observation, these sharp (narrow) fringes can be used to detect and measure surface irregularities as small as 10 Angstroms in height. Polished surfaces are found to be rough terrains whose hills and valleys vary in height and depth from 10 to 120 Angstroms. These small irregularities are not visible in the "double beam" interferometer of Figure 25.10 when surfaces S_1 and S_2 are of polished glass.

25.8.1.13 The interferometer method of Figures 25.9 – 25.11 is essentially a "contact" method. Experience and care are required in order to avoid undue scratching of one surface by the other. Life of the test glass is shortened by wear and scratching. A number of convenient interferometer techniques can be applied to testing flat surfaces without placing two surfaces in contact. However, existing interferometer methods for avoiding contact between two spherical surfaces are either so inconvenient to manipulate or so difficult to interpret that the contact method remains the standard method of the optical shop.

25.8.2 The Fizeau Interferoscope.

25.8.2.1 The Fizeau interferoscope, Figure 25.12, is a double beam interferometer that permits one relatively flat surface, S_1, to be tested against another flat surface, S_2, without placing these two surfaces in contact. The increased "working distance", d, is made possible without undue loss of contrast* in the fringes by restricting the effective size of the light source to a pinhole, H, and by illuminating the pinhole with monochromatic light. Since improved monochromaticity and smaller pinholes entail loss of light, the ultimate working distance, d, is restricted by the required level of illumination. Distances of d greater than 2cm must be considered "large" and should be avoided in designing and planning the interferoscope. Fizeau interferoscopes have been varied in design to meet the needs of various users. The use of beamsplitters as illustrated in Figure 16.2 is to be avoided in order to conserve light. The instrument illustrated in Figure 25.12 is an example of one of the more flexible types of interferoscopes. When this instrument is to be used for testing surface S_1 against surface S_2, the two sets of leveling screws, L_1 and L_2, are adjusted in the order mentioned so that the light beams reflected from S_1 and S_2 are refocused by the collimator as images of the pinhole, H, at the aperture, A. When the pinhole images formed at A are brought almost into unison by further relative adjustments on screws L_1 and L_2, straight fringes will appear on the observer's retina as he looks through the aperture, A, provided that the test surface, S_1, is optically flat. Interpretation of the interference fringes remains the same as with the simpler interferometers of Figures 25.9 and 25.10. Except for the more convenient and elegant manner in which the relative inclinations of surfaces S_1 and S_2 can be adjusted with the aid of the leveling screws, the procedures and methods of sections 25.8.1.3 - 25.8.1.5 apply again.

25.8.2.2 Many optical workers use the Fizeau interferoscope exclusively for ascertaining the degree of parallelism of the surfaces of a plane parallel plate. One surface, S_1, of plate, P_1, is first made optically flat. With interferoscopes of the type illustrated in Figure 25.12, test plate, P_2, is removed from table, T_2. The leveling screws L_1 are adjusted so that the two beams reflected from surfaces S_1 and S_{11} are focused within aperture A as images of pinhole, H. If both surfaces of plate P_1 are optically flat but are not quite parallel, the fringes are parallel to the line of intersection of surfaces S_1 and S_{11}. The fringes curve as surface S_{11} departs from flatness. As S_{11} is made optically flat and brought into parallelism with S_1, a single fringe of uniform intensity spreads over the field of view determined by the area of plate P_1. Equations (3) and (4) must be modified to include the refractive index n of plate P_1. Thus dark fringes occur when

$$nd = \nu \frac{\lambda}{2} \; ; \quad \nu = 0, 1, 2, 3, 4, \text{ etc.} \; ; \tag{5}$$

and bright fringes occur when

$$nd = \mu \frac{\lambda}{4} \; ; \quad \mu = 1, 3, 5, 7, \text{ etc.} \tag{6}$$

* See paragraphs 16.4 and 16.5 for the effect of monochromaticity, pinhole size and separation, d, on fringe contrast. Other principles underlying the use and interpretation of the Fizeau interferoscope are discussed in 16.2 and 16.2.2.

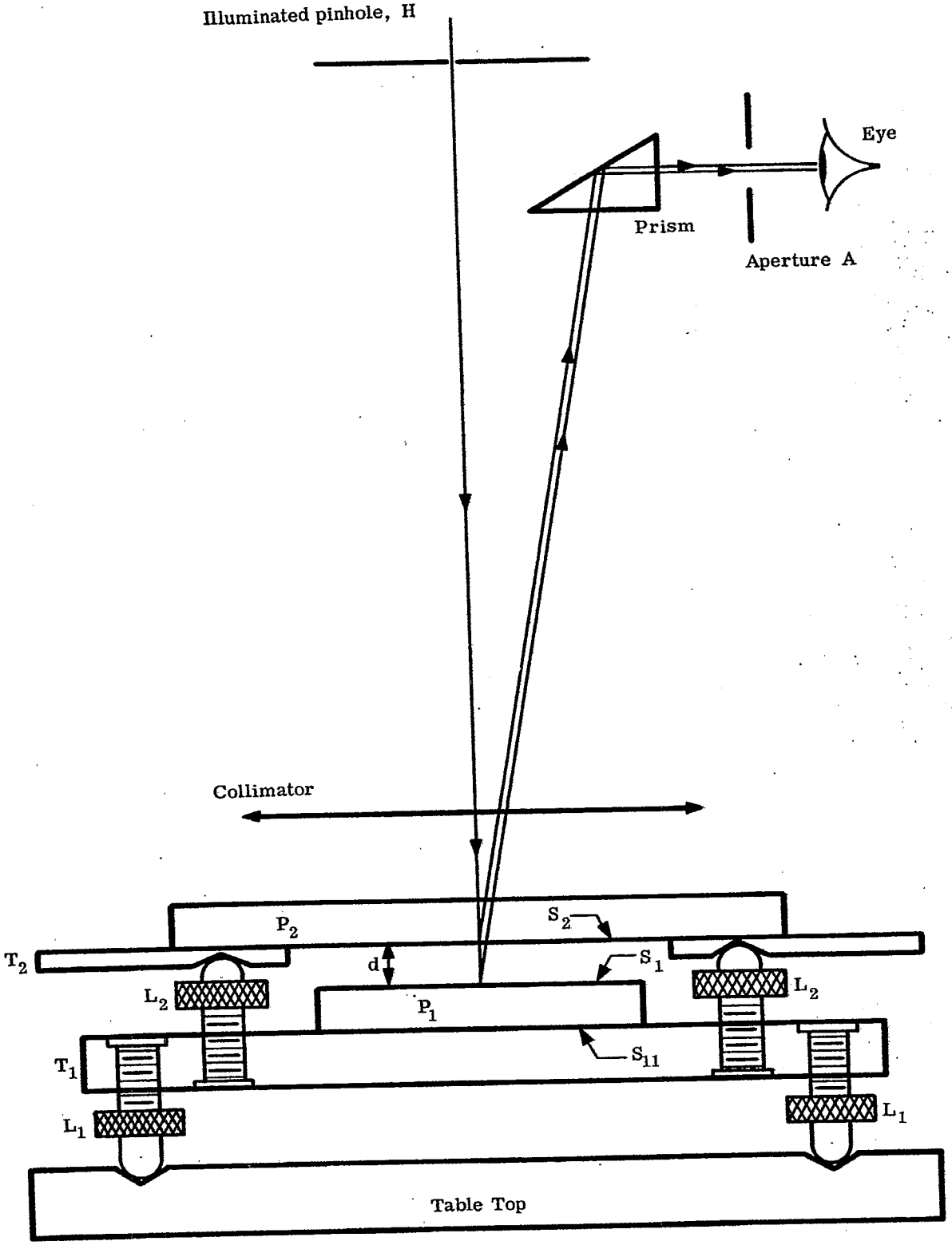

Figure 25.12 - A Fizeau interferoscope.

In other words, dark fringes occur when the optical path nd of the plate is equal to any integral number of half wavelengths, and bright fringes occur when the optical path is an odd number of quarter wavelengths. These conclusions can be expected intuitively when one considers that the phase change on reflection will be $\lambda/2$ at surface S_1, and 0 at surface S_{11}, so that the difference in the phase changes on reflection is $\lambda/2$. The beam reflected from S_{11} passes through plate P_1 twice, and thus is increased in phase by twice the optical path or 2(nd). Because the phase change on reflection is $\lambda/2$ at the air-to-glass interface, S_1, the two interfering beams proceed toward the observer with a phase difference, Δ, given by

$$\Delta = 2nd - \lambda/2. \qquad (7)$$

If now, nd is given by Equation (5), $\Delta = (\nu - 1/2)\,\lambda$ so that destructive interference takes place. But if nd is given by Equation (6), $\Delta = (\mu - 1)\,\lambda/2$. Since $\mu - 1$ must be an even number, $(\mu - 1)/2$ is an integer and Δ is an integral number of wavelengths. Hence we verify that constructive interference takes place when the optical path obeys Equation (6).

25.8.2.3 As an example of the sensitivity of the Fizeau interferoscope in testing for parallelism of the two surfaces of a plate, let us suppose that the diameter of the plate is 5cm, that its refractive index is 1.5, that the wavelength λ is 0.5461×10^{-3} mm and that the optically flat surfaces define a wedge whose optical path differs by $\lambda/2$ at the extreme ends of the wedge. Suppose that a bright fringe appears at the thin edge of the wedge. A bright fringe must appear at the thick end of the wedge since the optical path is greater by $\lambda/2$ at the thicker end of the wedge. This conclusion follows at once from Equation (6); for if nd is increased by $\lambda/2$, μ is increased to the next odd number, $\mu + 2$, the spectral order number of the next bright fringe, Equation (5) will be satisfied at the center of the plate so that a dark fringe occurs here. The field of the plate will appear very nonuniform. It presents one dark and two bright fringes. Despite this nonuniformity, the angle, α, between the surfaces of the plate is less than one second of arc. Since nd changes by $\lambda/2$ across the plate, the thickness of the plate changes by $\lambda/2n$. Therefore

$\alpha = \dfrac{\lambda/2n}{\text{diameter}} = \dfrac{0.5461 \times 10^{-3}}{3 \times 50} = 3.64 \times 10^{-6}$ radians or 0.75 seconds of arc. If the variation of intensity across the plate is reduced to 0.1 fringe, α will be reduced to 0.075 seconds.

25.8.3 A Modified Michelson Interferometer.

25.8.3.1 A flexible instrument, with the aid of which any surface (whether glass or metallic) can be tested for flatness against an optical flat without contact, is illustrated in Figure 25.13 as a specialized form of Michelson's interferometer. If S_1 is a surface of polished glass, surface S_2 is chosen as polished glass. If surface S_1 is metallic or high reflecting, an optical flat P_2 having surface reflectance approximating that of S_1 will be provided. The user can afford to supply several optical flats since these flats will not have to be replaced because of wear and scratches. The housing, H, is compact and rigid. It is designed to support the beamsplitter and the optical flat, P_2, with minimum vibration. The line OB is pointed in the vertical direction so that the test plate, P_1, is simply laid upon an auxiliary, stable support, Q. The arms OB and OA of the interferometer will be designed so that these arms are nominally of equal length and so that these arms are easily adjusted for equal lengths. Adjusting screws L can be utilized both for equalizing the lengths of the arms and for tilting surface S_2 with respect to S_1 to control the fringe width. The mechanism for tilting plate P_2 must be designed with great care because it is this mechanism that determines the operator's convenience in making quick and certain adjustments of the fringe widths as well as in checking arms OB and OA occasionally for equality by finding the "white light position". Supports Q should be ground to equal thicknesses in order to avoid hunting for the white light position each time Q is replaced by another support. An auxiliary, tiltable mirror M is provided for deflecting the light beam toward the observer.

25.8.3.2 Michelson's interferometer does not differ in principle from the interferometers of Figures 25.9 and 25.10. Consequently, the conclusions of paragraph 25.8.1.2 remain valid and the methods of paragraphs 25.8.1.3 - 25.8.1.5 apply again. Figure 25.14 illustrates why the Michelson interferometer behaves as the interferometers of Figures 25.9 or 25.10.

25.8.4 4 The Twyman-Green Interferometer.

25.8.4.1 The Twyman-Green interferometer is similar to the Fizeau interferoscope as regards basic principles* and interpretation. In both of these interferometers, the allowable optical path difference between the two interfering waves is increased by reducing the effective size of the source to that of a pinhole and by increasing the monochromaticity of the source of light. If, for example, mercury arcs are utilized, they should be operated at reduced pressure and followed by a high quality filter for 5461 Angstroms. The Twyman-Green interferometer has many points of mechanical similarity with Michelson's interferometer. However, Michelson's interferometer is invariably intended for use with broad sources of light.

* The principles underlying the Twyman-Green interferometer are discussed in paragraph 16.3.

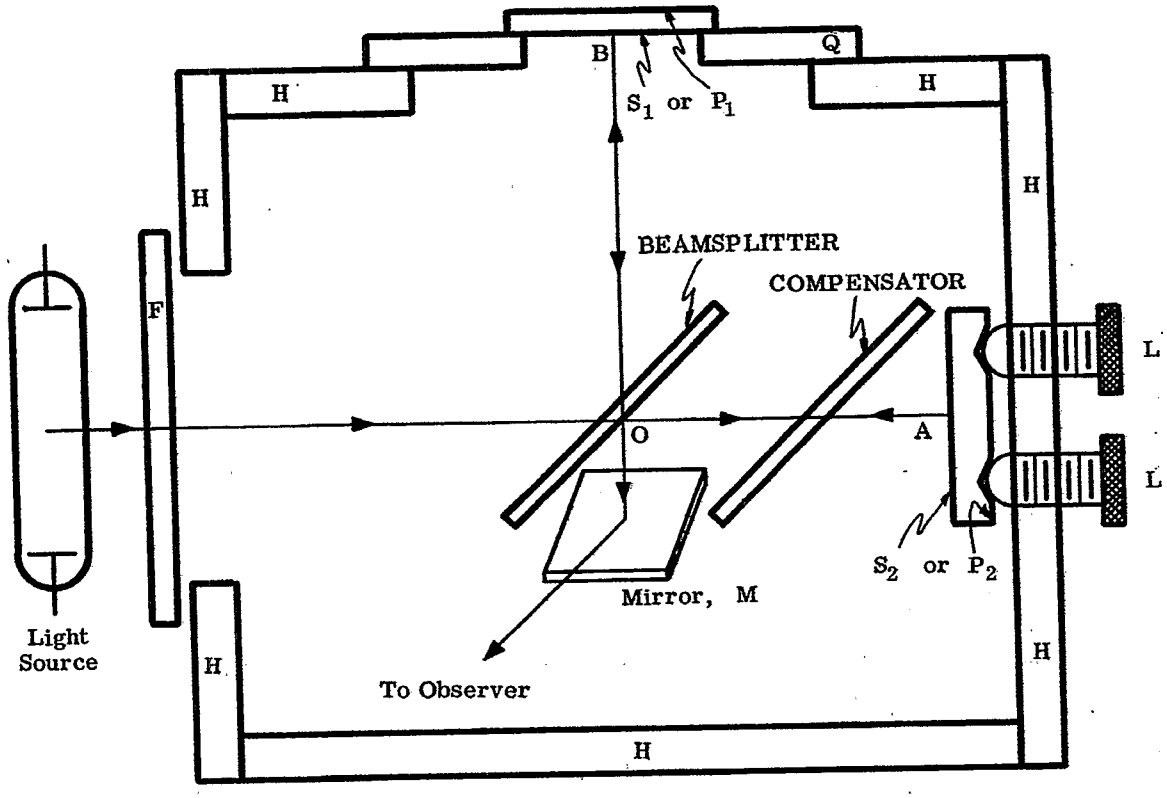

Figure 25.13- A modified Michelson interferometer.

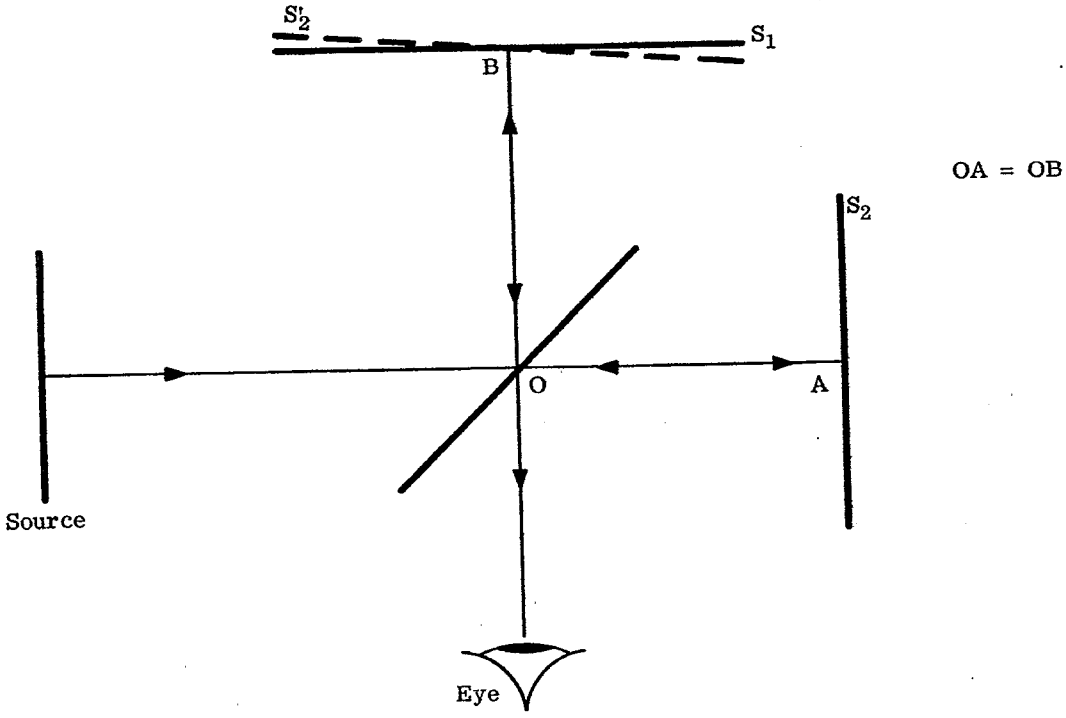

Figure 25.14- Michelson's interferometer as a method of Fizeau fringes. The observer sees surface S_2 as though it were located at S'_2, consequently, the fringes are formed as by reflection from two surfaces, S_1 and S'_2, that are in close contact.

25.8.4.2 Emphasis in the design of the Twyman-Green interferometer is placed upon taking advantage of the permissibly large optical path difference, d, between the two arms of the interferometer in measuring the variations of optical paths through plates or prisms. The instrument is not intended for regular use in checking flatness of surfaces. For maintaining best contrast in the fringes, the optical paths OA and OB, Figure 25.15, should be kept approximately equal. Accordingly, end mirror, M_2, is mounted on a slide that permits M_2 to be moved without appreciable wabble along the line AO. An iris diaphragm whose opening can be reduced to 0.75 mm, or less, in diameter is ordinarily used as pinhole, H. By means of this adjustable iris, the observer can choose his own compromise between brightness and contrast of the fringes. End mirrors, M_1, and M_2, are adjusted by means of suitable mechanisms (not shown) involving screws, L_1 and L_2, until pinhole images of H, formed after reflection at the end-mirrors, appear within aperture, A, at the rear focal plane of the telescope. If these pinhole images are not too far apart within A, fringes will be seen when the eye is placed behind A. One obtains the desired fringe width by further adjustments of L_1 and L_2. Failure to obtain good fringes as the pair of pinhole images is brought into unison indicates that the optical path difference between arms OA and OB is too great.

25.8.4.3 Figure 25.15 illustrates the arrangement for testing plates, P. Suppose that one knows that the surfaces of the plate are optically flat and that he wishes to check the uniformity of the optical paths through the plate. These optical paths can differ due to nonparallelism of the surfaces or due to nonuniformity in the refractive index, n. In one procedure the end mirrors, M_1 and M_2, are adjusted so that one fringe spreads over the field of view before plate, P, is inserted. The effects of introducing plate, P, are then observed. If the broad fringe is left practically undisturbed, the optical paths through the plate are sensibly uniform. The appearance of straight fringes indicates that the surfaces of the plate are not parallel. Irregularities in the fringes indicate that the refractive index is not constant. Let Δt and Δn denote variations in the thickness, t, and refractive index, n, of the plate, respectively, and let Δd denote the corresponding variation in the optical path difference, d, between the two arms of the interferometer. If Δn is negligible,

$$\Delta d = 2(n - 1)\frac{\Delta t}{\lambda} \text{ wavelength numbers.} \qquad (8)$$

If Δt is negligible,

$$\Delta d = 2\,\Delta n\,\frac{t}{\lambda} \text{ wavelength numbers.} \qquad (8a)$$

The factor, 2, enters because light waves traverse the plate twice. The following principles should be kept in mind.

(a) Each fringe is associated with a particular value of Δd.

(b) When one of the arms of the interferometer is altered in length by pressing upon the plate that supports the elements of the interferometer, each fringe moves such that Δd remains constant. With respect to the problem of interpreting the fringe system for the direction of the wedge that produces the straight fringes, one has only to shorten or to lengthen one arm of the interferometer and to note the corresponding movement of the fringes.

(c) In passing from one fringe to the next fringe of equal darkness or brightness, Δd changes by unity.

(d) In passing from a bright fringe to the next dark fringe, Δd changes by 1/2.

25.8.4.4 The base plate of the Twyman-Green interferometer is grooved or otherwise constructed so as to permit the end mirror, M_1, to be swung into orientations for testing prisms, etc. The configuration for testing right angled prisms is illustrated in Figure 25.16. Mirror, M_1, is adjusted for the desired fringe width. If all surfaces of the prism are known to be optically flat, the observed fringes reveal the degree of uniformity of the refractive index of the prism. More frequently, one will not have explored independently the degree of flatness of the surfaces of the prism. In such cases the observed fringes reveal the combined effects due to departures from surface flatness and due to inhomogeneities in refractive index. This method does not appear to have been modified to yield information about the angles of the prism or about deviation by the prism.

25.8.4.5 The following expedient is used, as the occasion demands, for distinguishing between effects due to inhomogeneity of refractive index and due to inadequate flatness of surface. The method is particularly effective in testing plates. As illustrated in Figure 25.17, plate, P, of Figure 25.15 is "immersed" between two optically homogeneous plates, E and F, that have outer surfaces of high degree of flatness. These plates are preferably, but not necessarily, plane parallel plates. For best results, the refractive indices of the immersion oil and of plates E and F should match the refractive index of the test plate, P. It can be useful to

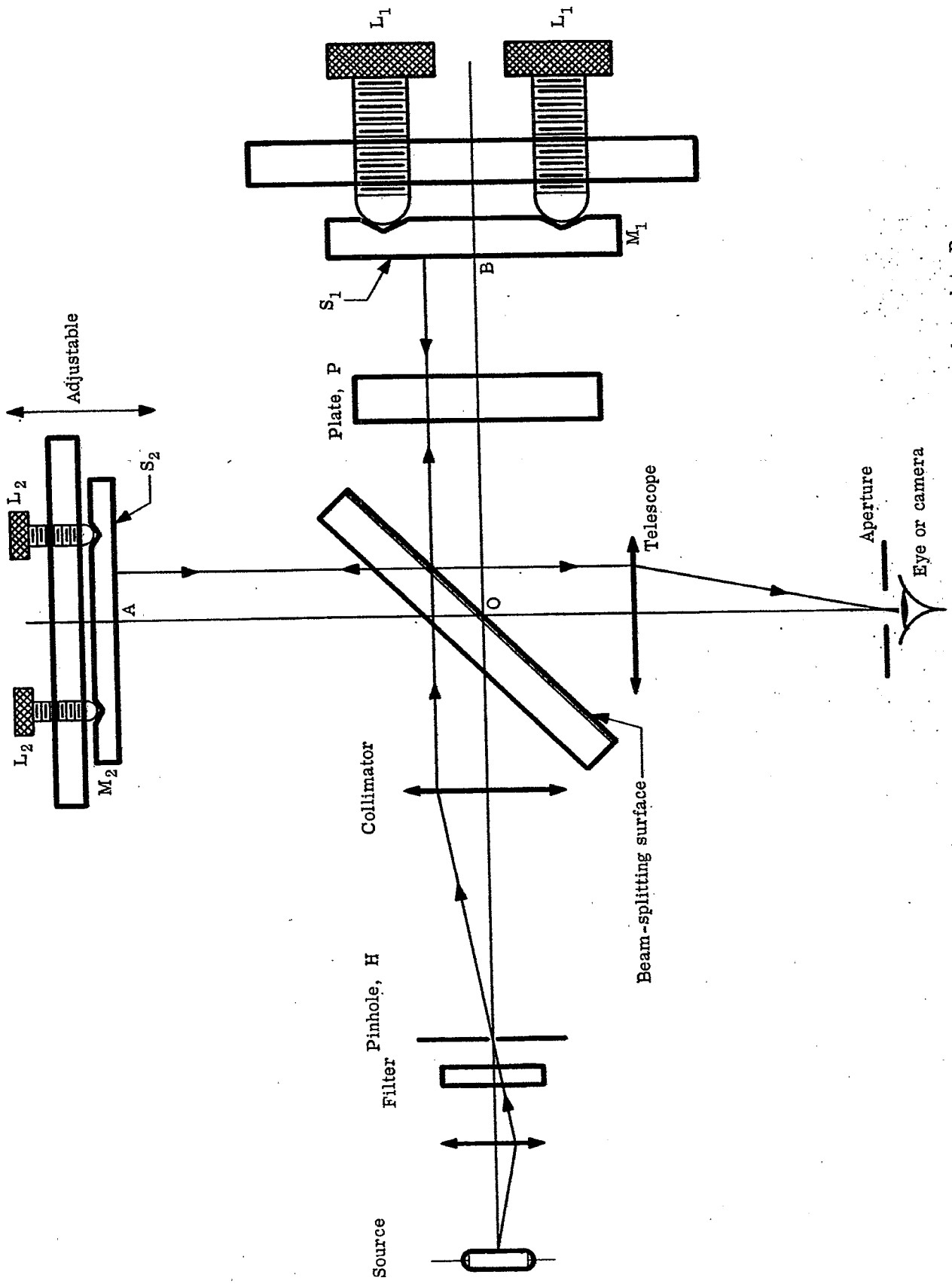

Figure 25.15- Twyman-Green interferometer as used for inspecting a glass plate P.

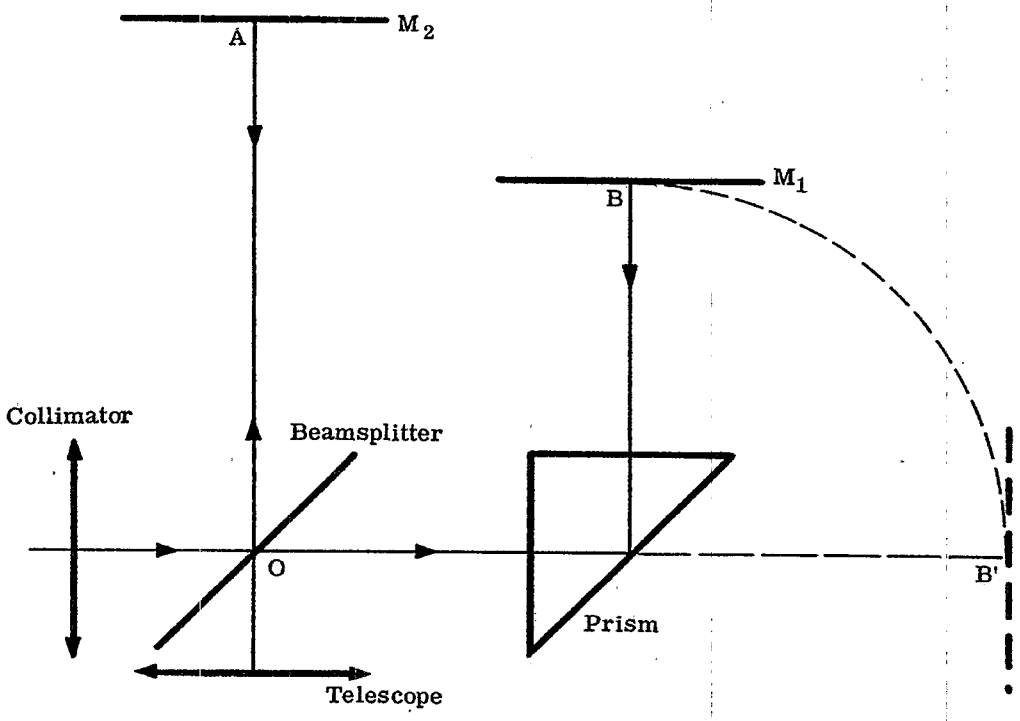

Figure 25.16- Modification of the location of end mirror M_1 for testing prisms in the Twyman-Green interferometer.

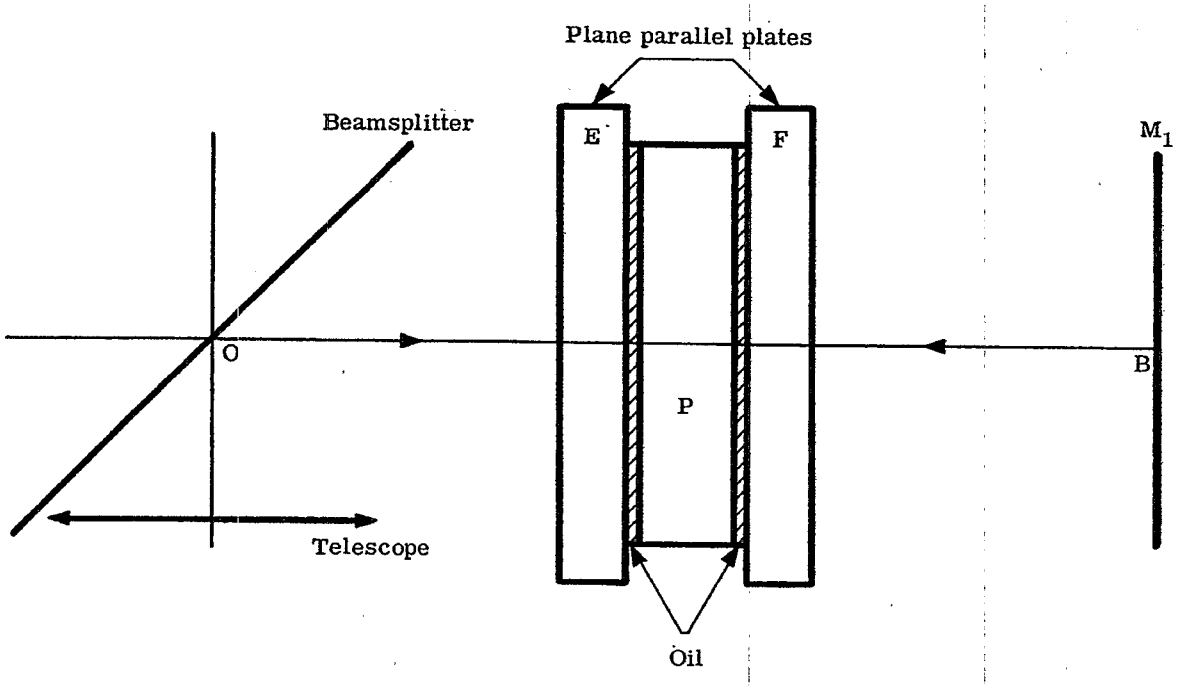

Figure 25.17- Method for obviating surface flatness of the test plate P.

"immerse" the prism of Figure 25.16 between two plane parallel optical flats. However, it is not possible to avoid lack of flatness at the reflecting surface of the prism.

25.8.4.6 Twyman-Green interferometers are provided, as illustrated in Figure 25.18, with an accessory fixture for observing spherical aberration of objectives throughout a wide range in focal lengths. Suppose that neither the collimator nor the test objective L possesses spherical aberration. Then rays from the axial point within pinhole, H, will be converged upon the axial point, C, at the rear focal plane of lens, L. If a spherical, convex mirror, M_1, is placed as indicated with its center of curvature at point C, all rays, ef, will be reflected back upon themselves and will emerge from lens, L, as normals to a plane wave that is propagated toward the beamsplitter. This plane wave interferes with the plane wave reflected from M_2 in the other arm of the interferometer to produce upon the observer's retina a family of straight fringes whose fringe width depends upon the angular adjustment of the end-mirror, M_2. In particular, a single fringe can be spread over the field of view. If the test objective has spherical aberration, all rays, ef, cannot be reflected back upon themselves. Consequently, the wave emerging from objective, L, will not be plane and will interfere with the plane wave from the other arm of the interferometer to produce interference fringes that display axial symmetry provided that the elements of objective, L, have axial symmetry and are well centered.

25.8.4.7 With objectives having long focal lengths, it is preferable to locate the convex mirror M_1 near the objective. This means that spherical reflectors having a series of radii should be provided. With objectives having short focal lengths, such as microscope objectives, the available working distance will not permit a convex reflector, M_1, but rather a concave reflector, M_1', centered about point C must now be used.

25.8.4.8 In actual practice, the exact location of the center of reflector, M_1, with respect to the axial point near the rear focal plane of lens, L, is problematical and becomes often a matter of choice. The spherical aberration can be less with respect to a focal plane that falls on one side or the other of the paraxial focal plane. Secondly, some consideration will show that the observed spherical aberration is not necessarily that of the objective alone. When the test objective has spherical aberration, the observed aberration is, in fact, the aberration of the combination consisting of the test objective, L, and the spherical mirror, M_1. Interpretation of the fringe displacements for the spherical aberration of the objective alone is not without objections of fundamental nature. But inspite of this difficulty, the Twyman-Green interferometer method is one of the better methods for indicating actual or relative amounts of spherical aberration in objectives of high optical quality.

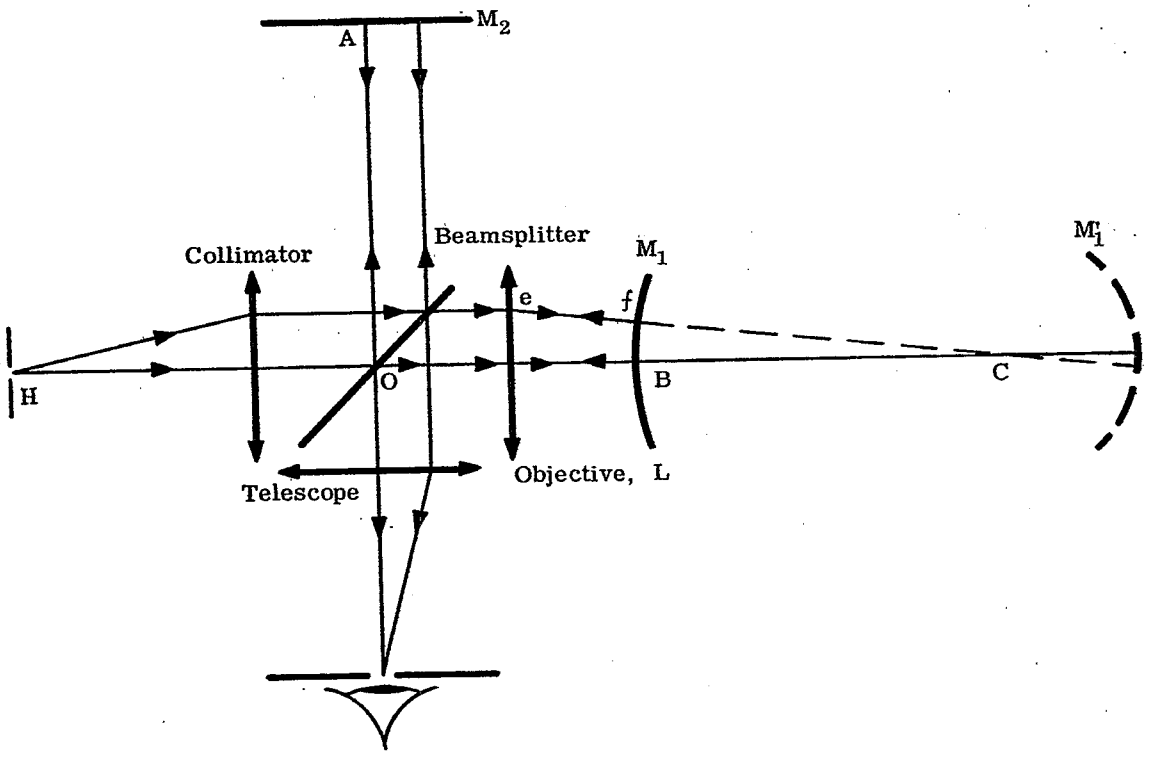

Figure 25.18- Adaptation of the Twyman-Green interferometer to the observation of spherical aberration of lenses, L.

25.9 THE RONCHI TEST

25.9.1 Introduction. One of the fairly common tests used currently by optical workers is the Ronchi Test [17]. This technique actually falls into a class known as the "shadow-fringe method". The geometrical aspects of the technique are outlined in Figure 25.19.

25.9.2 Theory.

25.9.2.1 The essence of the theory is as follows. Let us suppose as a start that a lens, L, produces a perfect star image at the paraxial focus, O, Figure 25.19. (The edge ray shown will not pass through B but through O.) Now if a plane grating of 4-8 lines/mm (Jentsch method 18 and 19) or 10-20 lines/mm (Ronchi method) is positioned at an arbitrary distance, g, from the focal point, O, as indicated in Figure 25.19, a shadow of it would be formed on a screen placed in a plane of projection arbitrarily distant p from O. Since we are, for the present, considering a perfect lens, rays from all parts of the lens aperture pass through O and this point is the single center of projection of the grating onto the plane of projection. Hence the shadow image of the grating has exactly the proportions, over all its area, of the grating itself, i.e. without distortion and with a constant magnification over its area of

$$\frac{\sqrt{\eta + \xi}}{\sqrt{y + x}} = \frac{p}{g} \qquad (9)$$

This ideal aberrationless case is usually not found and there is some spherical aberration, S, (shown for the edge ray in the figure) with the intersection points of other rays filling the space between O and B (simple undercorrection). Thus there is no longer a single point which can be considered as the center of projection for the entire grating. In this case the shadow image of the grating cast on the plane of projection will have a varying size scale over its area because centers of projection for points on the entire area of the grating lie between B and O. The magnification for any point on the grating becomes a function of the spherical aberration, S, of the ray passing through that point in accordance with the expression

$$\frac{\sqrt{\eta + \xi}}{\sqrt{y + x}} = \frac{p - S}{g - S} \qquad (10)$$

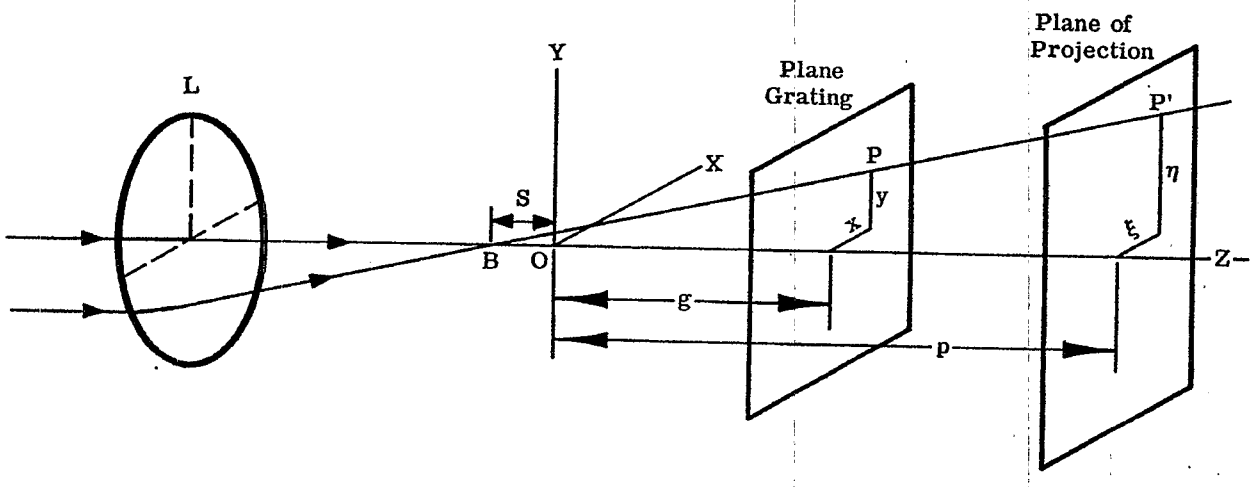

Figure 25.19-Geometrical theory of the Ronchi Test.
(After Martin's, Technical Optics, Vol. II, Pitman Pub. Co. 1950)

(17) Ronchi, Ann. d. R. Scula Normale Supriore di Pisa, Vol. XV (1923)
(18) Jentsch, Physikal Zeitschr, XXIX, 66, (1928)
(19) Martin, Technical Optics, Vol. II, 289, Pitman, 1950

If the grating is composed of straight lines its shadow image will show the lines as curved, and from the geometry of the figure, it can be shown that the curvature indicates the amount of spherical aberration present.

25.9.2.2 The complete theory must take into account not only the geometrical aspects outlined briefly here, but also the fact that interference may well be significant if the grating is as fine as those used by Ronchi or if more definitive interpretations are required. F. Toraldo Di Francia (20) has treated this subject in quite some detail, and the interested reader is urged to consult his paper.

25.9.3 Ann Arbor Tester.

25.9.3.1 There has appeared a commercial unit known as the Ann Arbor Tester based on this principal and manufactured by the Ann Arbor Optical Co. The tester is the device on the right of Figure 25.20.

25.9.3.2 The following Figures 25.21 and 25.22 are taken from the instruction booklet furnished with the instrument. Figure 25.21 [4(a)-(g)] shows the testing of an eight-inch focal length spherical mirror as a 175 line/inch grating is moved through focus on axis. Figure 25.21 [(5(a)-(d)] shows the patterns obtained with the Optical Tester and a thirty-inch focal length paraboloid cut 7° off axis. The pattern in [5(a)] shows the tester on the optical axis while [5(b)] shows the tester off axis; [5(c)] and [5(d)] were taken in the same positions but the parabolic mirror was rotated. The experimental arrangement is shown in Figure 25.22.

25.9.4 Jentsch's grid method. A similar testing technique using the coarser gratings of Jentsch is shown in Figure 25.23 taken from Martin (21) and showing the presence of spherical aberration. One optical shop checks all its work with this technique finding it a very sensitive and simple method for examing mirrors and lenses. The shadow - fringe method has much in its favor as an experienced worker gains a feeling quickly as to the nature of the defects of the system under test.

25.9.5 Summary. In the last analysis, however, all optical tests depend upon evaluation, and the experience of the optical worker himself is a vital factor. It is largely a matter of what the workers in a particular laboratory have previously used. One of the largest laboratories in the United States does practically no Ronchi-type testing as they have accumulated other equipment and know-how over the years that gives them the information they need.

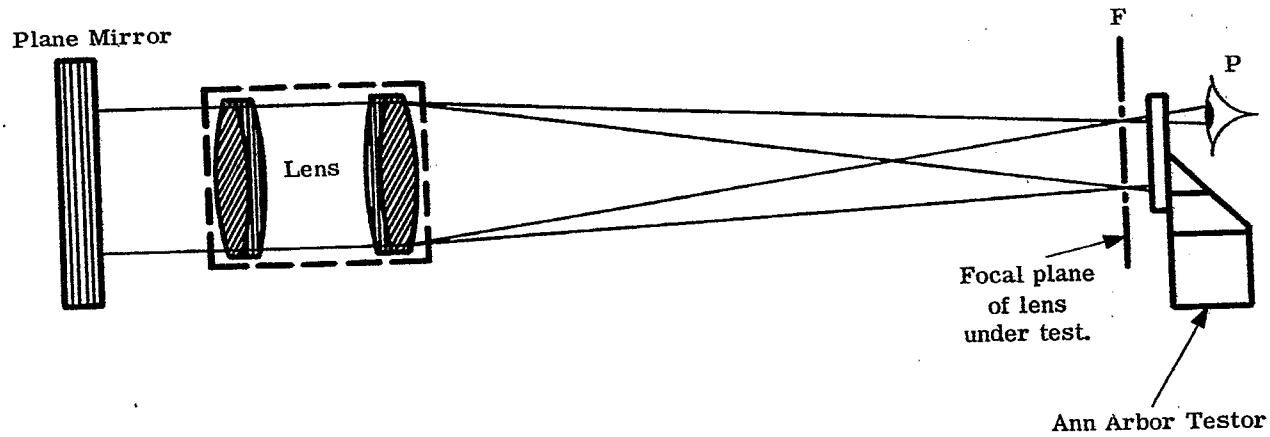

Figure 25.20 - The Ann Arbor Tester.

(20) di Francia, Optical Image Evaluation, (NBS Circular 526), 161, U. S. Gov't. Printing Office, (1954).
(21) Martin, Technical Optics, vol. 1, p289, Pitman, (1948). also Jacobs, Fundamentals of Optical Engineering. McGraw Hill, (1943).

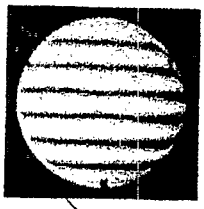

(a) -0.063"

(b) -0.031"

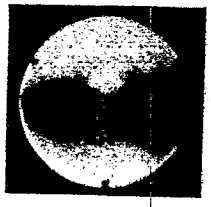

(c) -0.006"

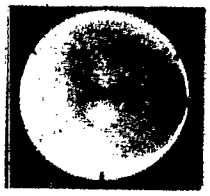

(d) 0.000"

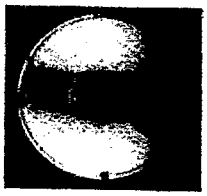

(e) 0.008"

(f) 0.025"

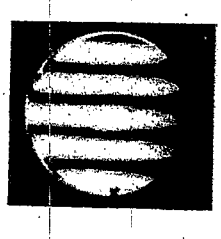

(g) 0.051"

Figure 4

(a)

(b)

(c)

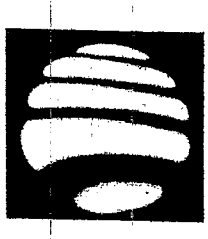

(d)

Figure 5

Figure 25.21- Patterns seen with the Ann Arbor tester for various optical systems.

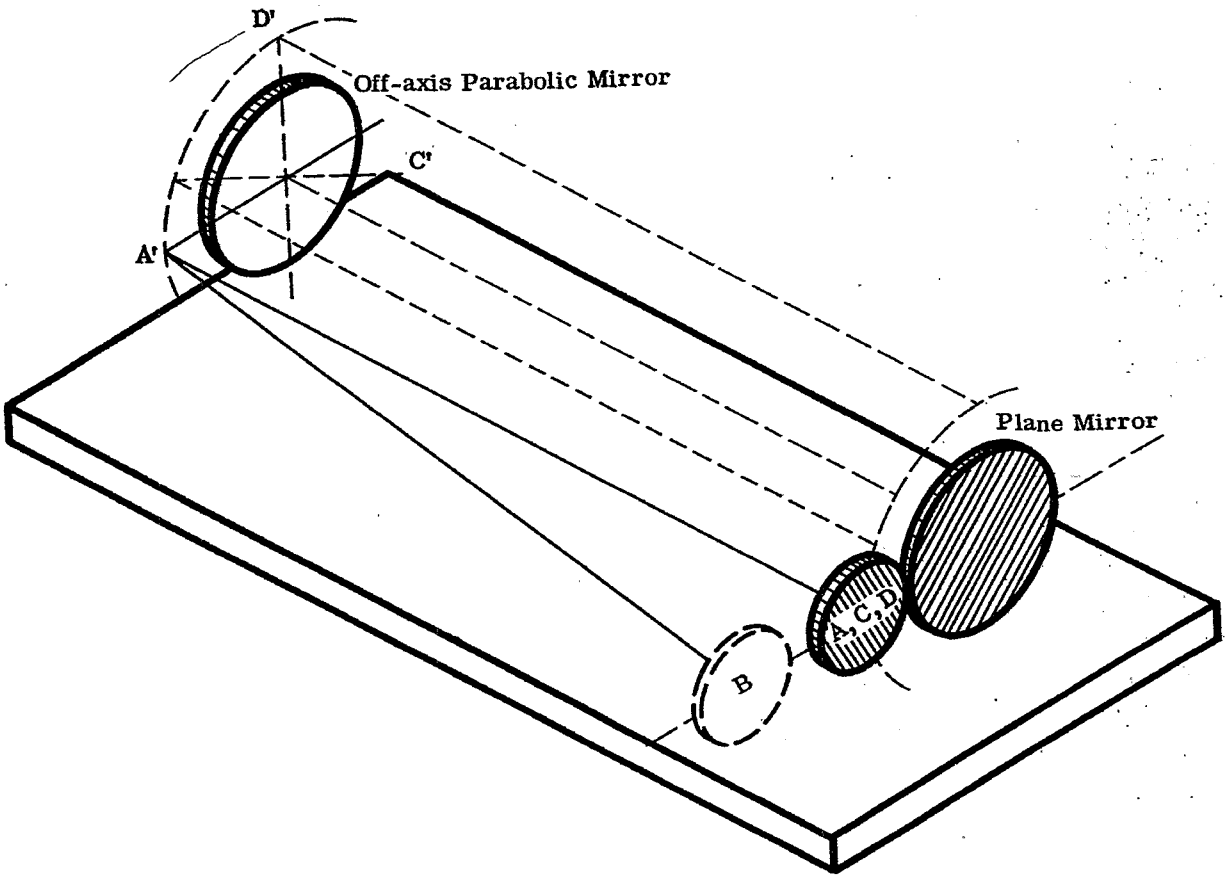

DETERMINING THE OPTICAL AXIS OF OFF-AXIS PARABOLIC MIRRORS

Often off-axis parabolic mirrors are received from the fabricator without markings indicating the side of the mirror which is toward the optical axis. Also, even with such markings, only the plane containing the axis is defined, and it is still necessary to locate the axis.

The position of the optical axis is easily determined by observing the pattern obtained with the Optical Tester. Only when the Tester is on the optical axis will the fringes be equally spaced and parallel to each other and to the lines in the grating when using an arrangement as shown in Figure 25.20.

The resulting patterns for the Tester in the correct and other positions with respect to the axis can be seen from the patterns pictured in Figure 25.21. Figure 5(a) in 25.21 shows the pattern obtained with the Tester on the optical axis of a 30" focal length parabolic mirror cut 7^{o} off-axis. This position is illustrated above, with the Tester at A and the edge of the parabolic mirror closest to the optical axis at A'. Figure 5(b) in 25.21 shows the pattern when the Tester, parabolic mirror, and plane mirror are still in the correct plane, but the grating is located outside the optical axis (B in the Figure above).

Figure 25.22- Determining the optical axis of off-axis parabolic mirrors with the Ann Arbor Tester.

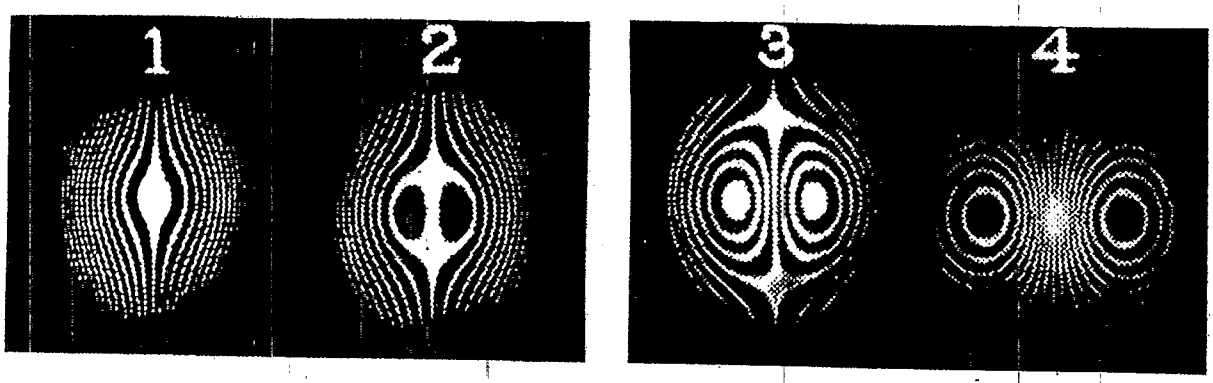

1 and 2 are shadow fringes outside the caustic. 3 and 4 are shadow fringes inside the caustic.

The appearances follow in the progression 1, 2, 3, 4.

Figure 25.23-Jentsch's grid method.
(From Martin's, Tech. Optics, Vol. II, Pitman Pub. Co. 1950)

25.10 FOUCAULT TEST

25.10.1 Introduction.

25.10.1.1 Having been given a lens or mirror surface prescription and having ground and polished the surfaces by hand or machine methods, the question arises as to what areas need to be "figured", i.e. be repolished to achieve perfectly the prescription. While helpful, the viewing of the image in toto is of less value than might be supposed, in that it represents the summation of the contributions from all parts of the surface. A technique which allows for inspection of the surfaces themselves is obviously required. One of the simplest and yet most delicate of all such techniques of surface testing was developed by Foucault (22) in 1859. The method requires, in its simplest form, merely a pinhole, a knife edge, the lens or mirror, and the eye of the observer. The system is shown diagrammatically in Figure 25.24 for a mirror.

25.10.1.2 In essence, the pinhole provides a small source of light which illuminates the surface of the mirror but which is so shielded that it sends no light directly into the eye. If we assume that the spherical surface is perfect and that the longitudinal aberration is negligible, then all rays striking the mirror will be focussed at some point, F. If the pinhole is located at the center of the curvature of the system, then F also will be at the center of curvature.

25.10.1.3 Assuming that the eye is placed close enough to the image so as to view the mirror in the Maxwellian sense (i.e. the eye receives all the rays coming to the focus), then the mirror surface will be evenly illuminated. (Actually even a perfect surface will show some deviations which will be discussed later.) If now a knife edge K is advanced in the direction indicated, the mirror surface will appear to go from completely bright to completely dark as the knife passes through F. Again for reasons to be discussed later this does not quite happen. If the knife edge is displaced toward the mirror from F then as it cuts into the beam the lower side of the mirror is darkened gradually and not until the beam is completely occulted will the eye see no light. If the knife edge is displaced from F away from the mirror, the reverse occurs. Clearly then the point where the intensity varies most rapidly with knife edge movement from bright to dark is the focus. If the knife edge always remains in the plane of the pinhole, then there will be only one place where the mirror darkens uniformly and rapidly with lateral displacement of the knife edge. This point is of course the center of curvature.

25.10.1.4 The extreme delicacy of this measurement will become more obvious if we study Figure 11.28 where a highly exaggerated error is present. Suppose there is an error of slope, angle, θ. The rays hitting

(22) Foucault, Ann de L'Obs. de Paris, V, 197 (1859).

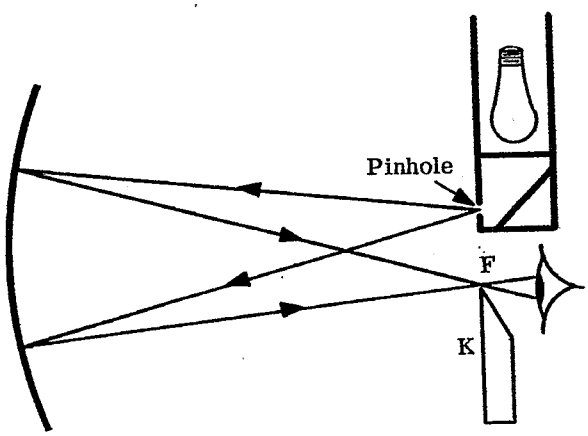

Figure 25.24- Experimental arrangement for a Foucault Test of a mirror.

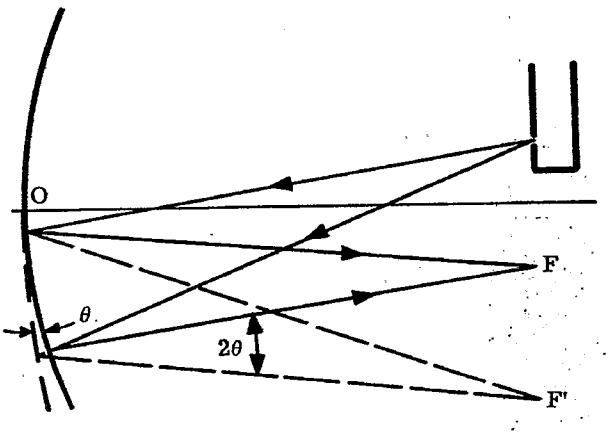

Figure 25.25- Schematic demonstration of sensitivity of Foucault testing.

this area will then be deflected from the correct focus by an angle of 2θ and the focal point for this area will be moved laterally a distance approximately equal to FO x 2θ. If the surface has a radius of curvature of ten and a slope angle error of 10^{-5} radian, then the deflection is 10^{-4} inches or .025 mm. An error this size on a lens of such small curvature would be barely detectable but on a larger focal length system it would be clearly visible. The test is actually so sensitive that slope angle errors of 10^{-6} radians are easily seen on the long focal length mirrors used in some telescopes.

25.10.1.5 Errors of this type usually appear as zones on the surface rather than isolated areas. Unfortunately while Foucault tests are very common, they are almost always done visually and few photographs are taken. The photographs of some drawings from Strong (23) are shown in Figure 25.26. The artistry of Roger Hayward, illustrator for Strong, clearly shows the variations in mirror illumination produced under the Foucault Test.

25.10.2 Detailed discussion of Foucault Test for spherical surfaces.

25.10.2.1 The preceding discussion has been highly qualitative and obviously over-simplified in some respects. To begin with the focus is never a pure geometrical point as we have demonstrated earlier. Secondly, the surface of even a "perfect" mirror does not appear all bright or all dark. It has been known for a long time that at the edge of a circular mirror there appears a very bright ring even when the knife edge has apparently cut through all of the rays. Banerji (24) has also observed that the surface for a real system with finite focal area does not grow continuously darker as the knife edge advances but rather the entire surface presents large variations in illumination. The peak illuminations get smaller and smaller until finally the whole surface is dark. Lord Rayleigh (25) attempted to explain the first of these two effects and was relatively successful. It remained for Zernike (26), Gascoigue (27), and recently Linfoot, in his articles and more recently in his book (28), to carry the interpretation of the Foucault patterns into the realm of the quantitative. Linfoot shows that the patterns may be determined analytically for an aberration-free system by assuming that electromagnetic waves originate at the surface being tested and combine according to the usual interference principles. In the event that the system is not aberration free, one must assume that the electromagnetic waves start at the pinhole and are reflected from the surface in the usual way.

(23) loc. cit., (7), 296,297
(24) Banerji, Astrophysical Journal 48, 50, (1918)
(25) Rayleigh, Phil. Mag. 33, 161, (1917)
(26) Zernike, Physica 1, 689 (1934)
(27) Gascoigue, M. N. 104, 326, (1945)
(28) Linfoot, Recent Advances in Optics, 128 at req. (1955) Oxford

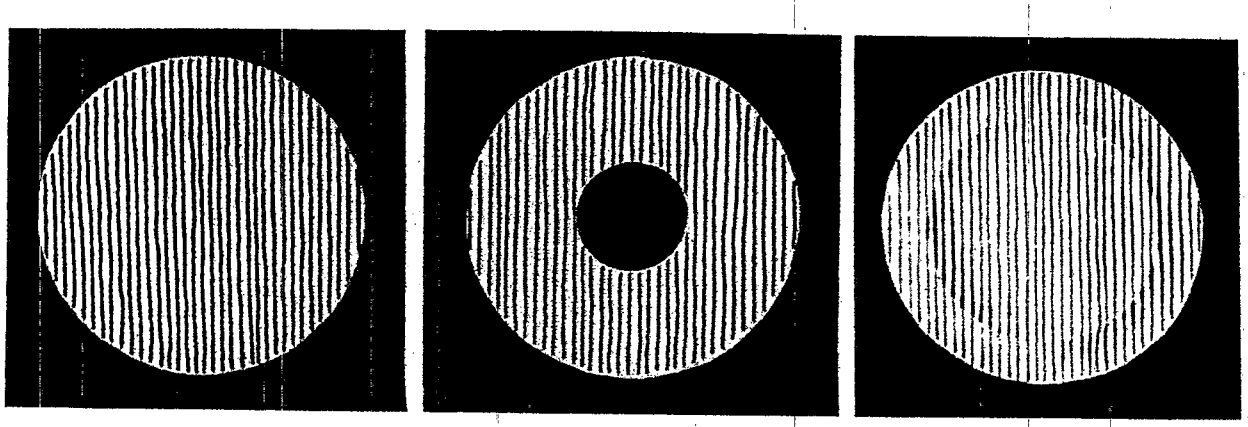

(a) Spherical mirror tested at the center of curvature.

(b) Parabolic mirror tested with a flat testing mirror.

(c) Spherical mirror with a raised annular ridge as tested at the center of curvature.

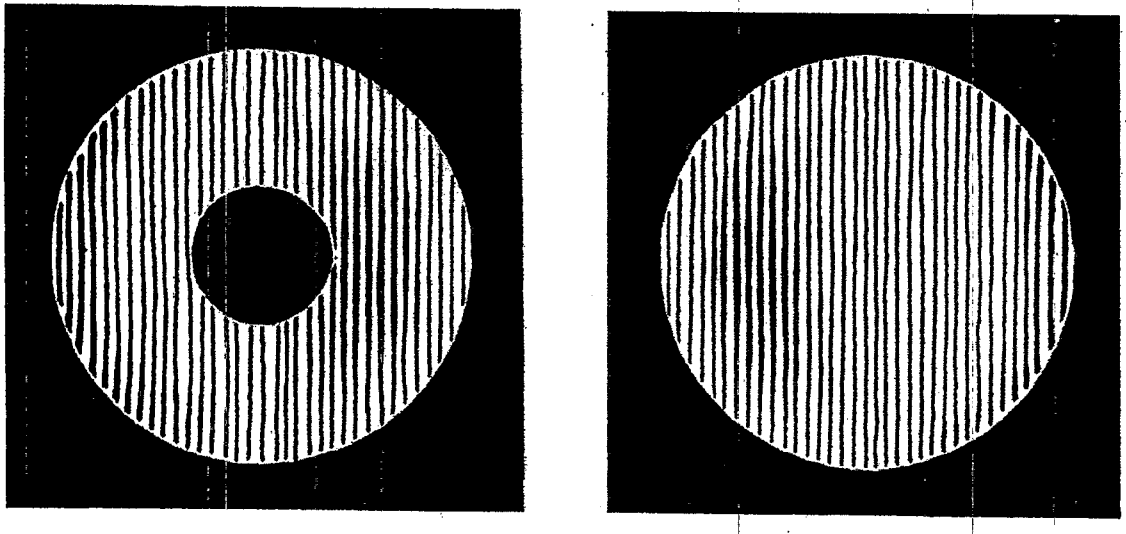

(d) Spherical mirror tested with a flat testing mirror.

(e) Parabolic mirror tested at the mean center of curvature.

Figure 25.26-Foucault test appearances.
(From Strong's, Procedures in Experimental Physics, Prentice-Hall Inc., 1938)

25.10.2.2 Linfoot concludes that the variation of illumination, D(x', y'), of the knife edge is given, to a good approximation, by the equation

$$D(x', y') = \frac{1}{2\pi} \int_0^{\infty} du \int_{-\infty}^{+\infty} e^{(-iux' - ivy')} W(u, v)\, dv \qquad (11)$$

Where

$$u = \frac{2\pi x_1}{\lambda s}$$

$$v = \frac{2\pi y_1}{\lambda s}$$

$$i = \sqrt{-1}$$

s = distance from the vertex of the surface to the knife edge.

$$W(u, v) = \frac{1}{2\pi} \int \int E(x, y)\, e^{(iux + ivy)}\, dx\, dy$$

E(x, y) = illumination over the surface

Note carefully that (x, y) represent coordinates of a point on the surface under test; (x_1, y_1) represent the corresponding coordinates in the plane of the knife edge; and (x', y') represent the corresponding coordinates in the image of the x_1, y_1 plane.

25.10.2.3 An application of this equation to a true mirror with knife edge central gives Figure 25.27 (from Linfoot). Here the brilliant zone around the edge of the mirror is clearly predicted.

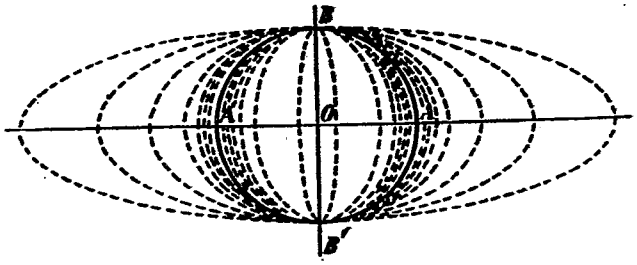

Isophotal lines for a true mirror under the Foucault test, with the knife edge central.

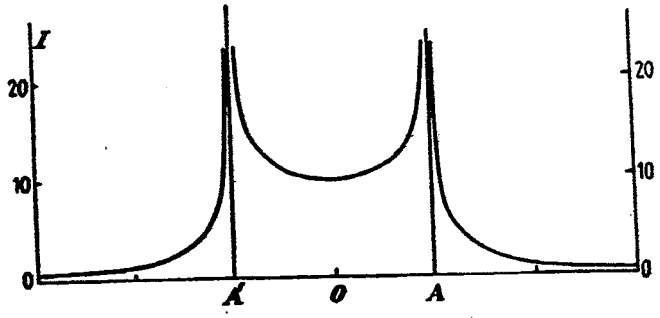

Intensity distribution along the horizontal diameter (after Linfoot).

Figure 25.27 - Isophotal lines and intensity distribution for a mirror under the Foucault test (From Linfoot's, Recent Advances in Optics, Oxford Univ. Press, 1955)

25.10.2.4 If the knife edge is kept in the central plane but moved a distance, C, laterally we see the oscillations of Benerji (29). In this diagram $C' = \frac{2\pi C}{\lambda S}$, where C' is the distance moved in the plane of the image of the knife edge.

25.10.2.5 A practical problem frequently occurs in using the Foucault Test for surfaces of low reflection. The small pinhole that must be used results in very low light intensities, and the low light intensities make detection of the Foucault shadows difficult. To improve the situation a slit may be used. The slit must not only be narrow, but also of a length such that the aberrations of the system under study are effectively constant over this length. The details for interpreting the pattern resulting from this type of source are given in Linfoot (30).

25.10.3 The Foucault Test applied to non-spherical mirrors.

25.10.3.1 The Foucault Test can be used for paraboloidal as well as spherical mirrors. To simplify the interpretation, an additional flat is required as shown in Figure 25.28. For paraboloidal mirrors one may use several modifications of the basic Foucault test. One employs a flat mirror with a hole in the center. The arrangement is equivalent to that shown, but the observer looks along the axis of the surface being tested.

25.10.3.2 Another modification is the technique developed by Gaviola (31). This method is more sensitive than the basic test and is particularly useful as a guide in very close control of zonal errors. The experimental arrangement is shown in Figure 25.29. The Gaviola technique depends on the fact that for off-axis areas of a paraboloid the positions of best focus do not lie on the center line of the paraboloid but rather lie on a caustic which originates at the center of curvature. The method is essentially as follows. First the paraxial focal point is determined by the regular knife edge method. From this datum the equation of the caustic for the non-aberrated paraboloid is calculated. Next one calculates where the center of curvature (ξi, n_i) should be for a given facet or area. A knife edge is then used to determine where the center of curvature actually is - all of the paraboloid except the facet in question being covered up. The deviations $\Delta\xi$, Δn_i of the actual center of curvature from the ideal center of curvature for various facets are used to map the true surface of the mirror. Symmetry about the center line is assumed.

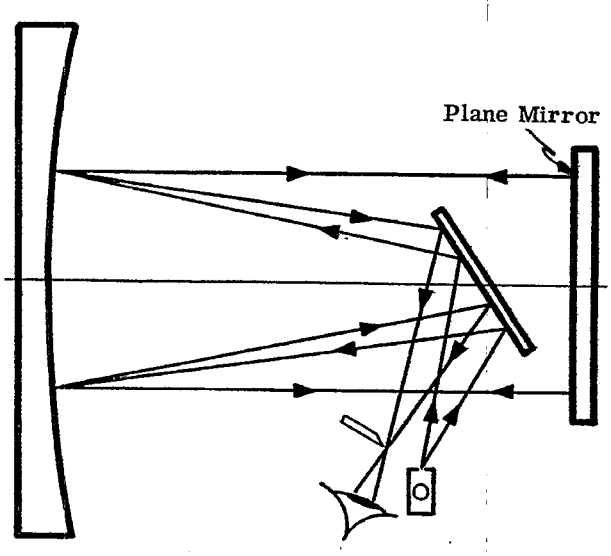

Figure 25.28- Foucault Test set-up for paraboloidal mirrors.

(29) loc. cit., (24)
(30) loc. cit., (28), 146
(31) Gaviola, JOSA 26, 163 (1936); also Strong, loc. cit., 23, p. 298

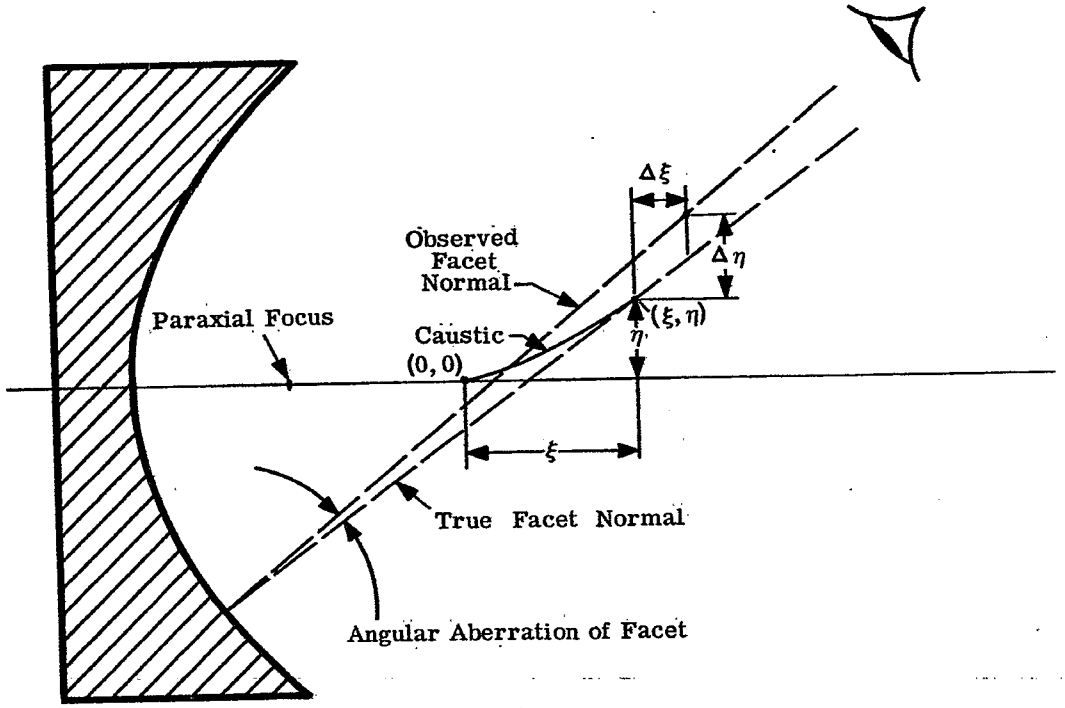

Figure 25.29-The Gaviola technique of Foucault Testing.

(After Strong's, Concepts of Classical Optics, W. H. Freeman and Co. 1958)

25.10.4 The Foucault Test applied to lenses. The previous discussion may have left the impression that the Foucault test is really applicable only to mirrors. This is not so. Basically any type of system may be tested with the same advantages accruing. Several examples are given in Strong (32) . The essential technique is the same in each instance with modifications made as dictated by the system under test. In each case, it is the possibility of inspecting the zonal contributions more or less individually rather than seeing them in their integrated form which makes this test so important. Recently one of the leading precision optical makers commented that due to the increasing use of aspheric surfaces, virtually all of his lenses and mirrors were tested by this method.

25.11 THE STAR TEST

25.11.1 Introduction. It has been pointed out before that the choice of optical testing technique is frequently strongly related to the individual and his particular experience. It is generally acknowledged that H. Dennis Taylor carried the star test to its present heights and his disparaging comments on the knife-edge, or Foucault, test are interesting to read (33).

25.11.2 Technique.

25.11.2.1 The star test, as practiced by Taylor actually used a star as source of parallel light. The most frequently used star was Polaris although for checking achromatism, he also used the bluish star, Vega, and the reddish star Orionis. Today with the press of work, etc., it is seldom practical to depend on the visibility of the night sky, and artificial stars are used. One of the best "stars" is made by piercing a needle point, well honed, to varying degrees into layers of very thin tinfoil backed up by something like a very hard plastic or ebonite. Several trials should result in a very small perfectly round hole. The resulting aperture is then illuminated by a Pointolite lamp or equivalent and placed at the focus of a well corrected collimator as shown in Figure 25.30. Without much doubt, one of the best collections of star test photographs appears in Taylor's book and repeated also in Twyman's (34). It is reproduced in Figure 25.31. For convenience reference will be made using the figure numbers that appear in the photograph from Taylor, following in parentheses our figure number e.g. Figure 25.31(10a) is Taylor's Figure 10a, etc.

(32) Strong, Procedures in Experimental Physics 70-72 Prentice Hall (1953)
(33) Taylor, The Adjustment and Testing of Telescope Objectives, 50, Grubb, Parsons and Co. (1946)
(34) Twyman, Prism and Lens Making, 369, Hilger (1957)

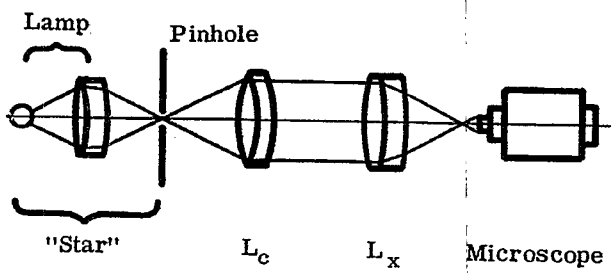

Figure 25.30- The experimental arrangement for a star test.

25.11.2.2 The star test technique consists of examining the image of the star with a fairly high power magnifier or telescope. It is pointed out clearly by Taylor that a careful examination of the observer's own eye is mandatory if a correct analysis of the system under test is to be obtained. The tests such as rotating the objective are simple to make. If the astigmatism rotates with it, the fault is with the objective, if not, the fault is with the eye.

25.11.2.3 In most instances more information is to be gained by examining the image out of focus and watching what happens as it goes through focus than trying to evaluate the system by an examination of only the in-focus image. The perfect figure will expand concentrically in an even fashion as the image passes through focus, with the intensity varying regularly in the ring structure. A perfect lens is shown in Figure 25.31(17) while Figure 25.31 (18) shows the variation as a well-corrected lens passes through focus. It will be instructive to consider the principal star tests in the manner of Taylor, and this will now be done with frequent reference to Figure 25.31.

25.11.3 Squaring-on.

25.11.3.1 A telescope objective is considered "square-on" when the optical axis of the objective passes directly through the center of the axis or stated another way -- when the optical axis of the objective and the eyepiece coincide. Should the objective be cocked with respect to the eyepiece, the appearance of the image will depend upon the residual aberrations in the objective (assuming the eyepiece is effectively perfect). Usually the aberrations at focus that distort the image will be coma and astigmatism. Such a system is shown in Figure 25.31 (10a).

25.11.3.2 Reference should be made to Taylor for the actual process of squaring-on the objective, but the principle is clear from the photographs, viz. that the incorrectly adjusted objective will result in even the best focus being non-symmetric. Further, as the eyepiece is racked through focus, the image does not expand concentrically about the best focus image, but does so about a point to one side of the best focus image.

25.11.4 Achromatism.

25.11.4.1 It is a fundamental principle of instrumentation that we are interested in the performance of the whole instrumentation system and not just a part of it. Thus with visual optics and the known defects of the eye, we must design systems that take these defects into consideration. Occasionally we can put the defects to good use, but at all times we must be conscious of their effect upon the rest of the system. Even a perfect reflector

will show a colored star test visually because of the achromatism of the eye. This may be checked easily and due account taken of it in judging systems whether they be reflective, refractive, or a combination thereof.

25.11.4.2 The defects of the eye are of course involved in the choice of eyepiece with which to judge the objective. Usually a fairly high power objective with a magnifying power of 50 - 100 times is suitable for use with a well-corrected eyepiece. Lower power objectives involve more of the eye aperture and consequently are affected more by the achromatism of the eye.

25.11.5 Astigmatism.

25.11.5.1 The nature of astigmatism has been discussed elsewhere in this manual so its details will not be reworked. It suffices one to say that the aberration known as astigmatism results in a star being focussed into two "lines" that are at right angles to each other, and displaced by an amount that depends upon the angle of view. This aberration is very easily detected with the star test. As the eyepiece is racked through focus one might see the image vary as in Figure 25.31 (12 d, d", d'). For corresponding positions inside and outside of focus one might see images as in Figures 25.31 (13) and (14).

25.11.5.2 A study of the photographs in Figure 25.31 and of the aberrational theory indicates that the star test is indeed a marvelously simple, and yet accurate, method for testing for astigmatism. It must be understood that seldom will a system have just one aberration and that particularly as one goes off axis, it becomes increasingly difficult to stipulate exactly the cause of the image degradation. It is here that experience plays such a vital role.

25.11.5.3 Assuming in the present case that only astigmatism is involved, one will usually find that the position of best focus will show a roughly circular image - the disk of least confusion - half way between the two astigmatic focal lines and of a diameter approximately equal to one-half the length of either focal line. While astigmatism is not as bad an aberration as some, if one is interested in "pointing" because of its symmetry, it may increase the spot diameter several hundred percent. This clearly decreases the resolution possible with the system. Once again we call the attention of the reader to the fact that the requirements of a good pointing system are not as stringent as those for a system of high resolution. This fact is too often overlooked.

25.11.5.4 As previously indicated, the defects of the eye must be taken into account and a truly stigmatic system may appear to the eye to be astigmatic. It is not only possible to separate the astigmatism of objective, eyepiece, and eye, but careful design can result in a system that shows no astigmatism to the eye, yet each component of the system, objective, eyepiece, and eye, each have demonstrable amounts of this aberration. Again the tests of the eye should be made initially with a low power eyepiece. More detailed drawings of star effects showing astigmatism, after Zernike and Nienhuis (35) are shown in Figure 25.32.

25.11.6 Zonal and marginal spherical aberration.

25.11.6.1 Perhaps the best way to get a feel for how the star test demonstrates zonal and marginal spherical aberration is to refer to Figure 25.33 where three possible extremes are depicted: (a) no spherical (b) marginal spherical and (c) zonal spherical. In each instance the lens under test (the element could of course be a mirror, etc.) is directed toward a distant star or equivalent as previously explained. In case (a) there is no spherical aberration at all and geometrically all rays come to point focus. Actually of course interference spreads the point into the familiar interference pattern and such a lens would show a perfect figure such as Figure 25.31 (17) at focus. Either side of, but not far from focus, such a lens might produce images such as Figure 25.31 (22) and (23). A glance at Figure 25.33 (a) demonstrates why this is so.

25.11.6.2 If the lens has marginal spherical aberration but little or no zonal, then we might see within focus an image similar to that in Figure 25.31 (15). Note carefully that there is no very bright center as contrasted with Figure 25.31 (22). Note also the way the intensity of the rings varies with transverse distance. Figure 25.31 (15) shows positive marginal spherical, i.e. the edge rays come to focus between the paraxial focus and the lens. Figure 25.31 (15a) shows negative marginal spherical aberration. The reason for Figure 25.31 (15) is again clear by reference to Figure 25.33 (b). Within focus there is a greater concentration of light for the marginal than for the central rays.

25.11.6.3 Where the marginal spherical aberration has been corrected, there may be residual zonal. This manifests itself, as might be expected, by an image of the form of that shown in Figure 25.31 (20) (inside focus) and 25.31 (20a) (outside focus). That there should be this high concentration in the third and fourth rings inside focus and in the 2 and 3 and 5th rings is reasonable providing the zonal error is as shown in Figure 25.33 (3c).

25.11.6.4 When checking for zonal or marginal spherical, the best technique is to check through focus and not just at focus. Further, the inspection should be made far enough from focus so that several rings appear as this is a more sensitive test. Generally speaking, the rules for interpreting zonal spherical aberration are

(35) loc. cit., (26), 96, Plate V

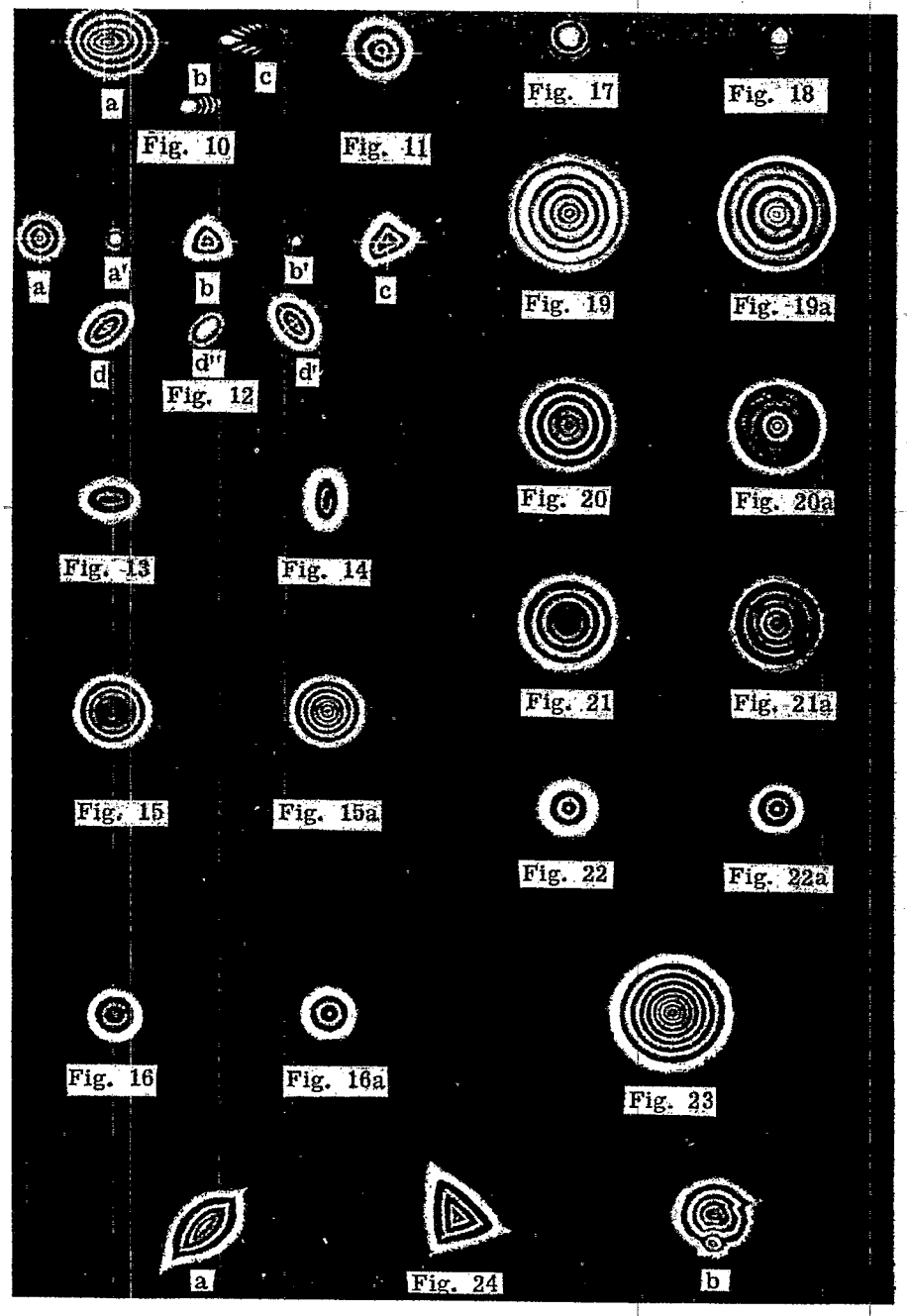

Figure 25.31-Star testing. (From Taylor's, The Adjustment and Testing of Telescopes Objectives, Grubb, Parsons and Co. 1946)

Fig. 10a.- Eccentric appearance of interference rings, due to the objective being out of adjustment.
c.- The focussed image of a star, when the maladjustment is about as much as in the last case.
b.- The focussed image, as visible when the objective is moderately out of square.
Fig. 11. - A section of the cone of rays taken closer to the focus, exhibiting a more moderate degree of maladjustment.
Fig. 12. - a, b, c, d, and d' are out-of-focus sections, as will be seen when the objective is correctly "squared on," and quite irrespective of other faults.
a', b' and d" are appearances of the focussed image corresponding respectively to a, b and d.
d, d and d" are also examples of astigmatism.
Fig. 13. - A section taken a very little way within focus, under a high power, exhibiting the fault of astigmatism.
Fig. 14. - The corresponding appearance to Fig. 13, as shown by a section taken at the same distance beyond focus.
Fig. 15. - Section within focus, showing result of positive spherical aberration.
Fig. 15a.- The corresponding section, taken at the same distance beyond focus.
Fig. 16. - A section taken closer to focus under a high power, exhibiting a slight residual spherical aberration; the central rings rather weak.
Fig. 16a.- The corresponding appearance at the same distance beyond focus; the central rings relatively strong.
Fig. 17. - The spurious disc or image of a star yielded by a perfect objective, and viewed under a very high magnifying power.
Fig. 18. - The spurious disc sometimes yielded by a large objective when resting upon three points, without intermediate supports being supplied to counteract the flexure due to the weight of the lenses.
Figs. 19 and 19a.- An example of marked zonal aberration, being sections of the cone of rays taken inside and outside of focus respectively.
Figs. 20 and 20a.- Another example of zonal aberration.
Figs. 21 and 21a.- Example of the general figure of an objective being tolerably good, but there is a region in the centre having a focus somewhat beyond the main focus.
Figs. 22 and 22a.- Two sections of the cone of rays yielded by a perfect objective, taken very near to and on opposite sides of focus. and viewed under a high power.
Fig. 23. - A section of the cone of rays yielded by a perfect objective, taken at about 1/4-inch on either side of focus, and viewed under a moderately high magnifying power.
Figs. 24 and 24a.- Examples of violent mechanical strain, due to imperfect mounting or bad annealing.
Fig. 24b.- Example of the effects due to the presence of veins in the material of the objective.

Index to Figure 25.31
(From Taylor's, The Adjustment and Testing of Teles. Objectives, Grubb, Parsons and Co., 1946)

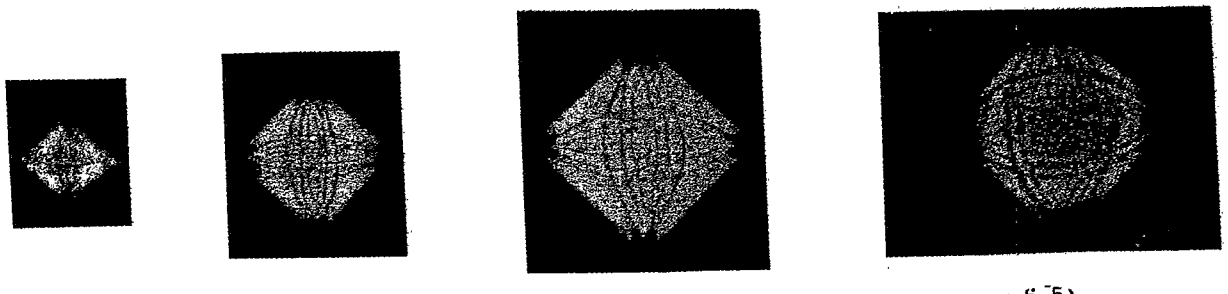

± 1.4λ ± 2.7λ ± 3.5λ ± 6.5λ

Figure 25.32-Star tests showing astigmatism of varying degrees.
(From Linfoot's, Recent Advances in Optics, Oxford Univ. Press, 1955)

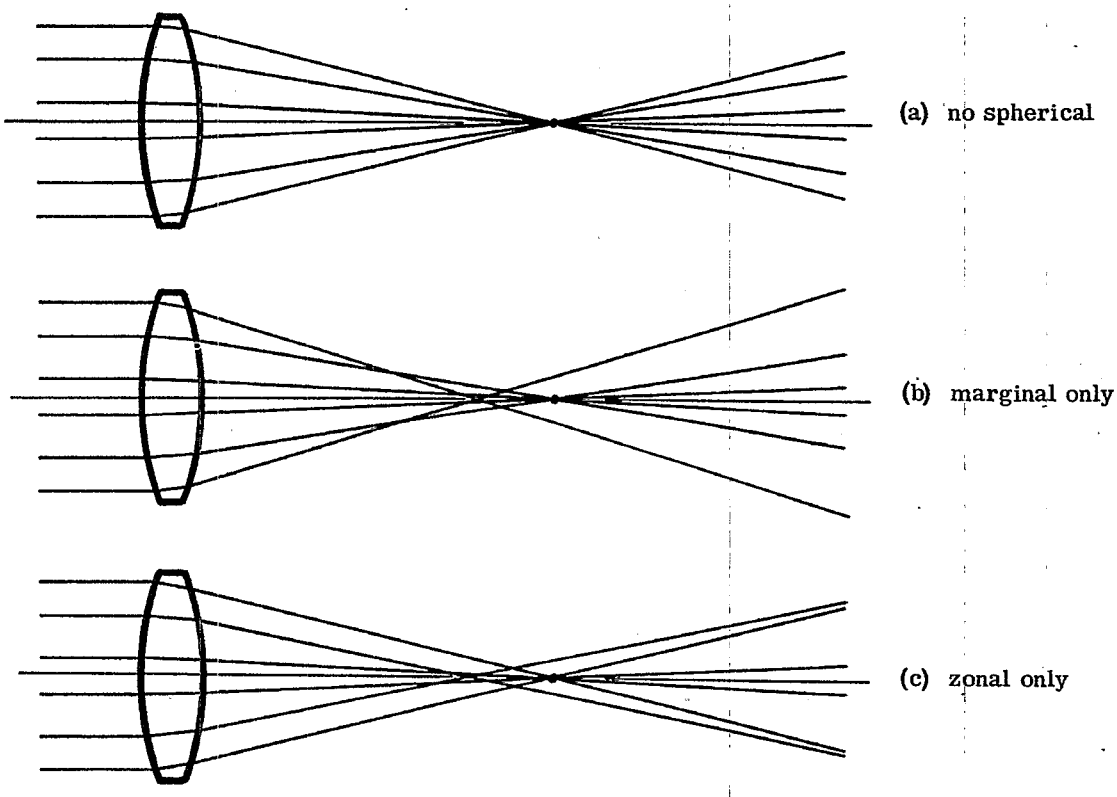

Figure 25.33- Various types of spherical aberration.

fairly straightforward with a bright zone or ring inside focus corresponding to a zone that focusses short. A bright zone or ring outside focus corresponds to a zone that focusses long. This corresponds of course to positive and negative zonal aberration. Again, Nienhuis (36) gives somewhat more detailed data, but not quite as much general information as Taylor. Figure 25.34 shows star images with varying degrees of primary spherical aberration at various focal positions.

25.11.6.5 It is clear that the star test furnishes a sensitive measure of the integrated effect of the whole lens. There is some question as to whether it gives as much information about a specific part of the lens or mirror as might a Foucault Test.

25.11.7 Coma. A good photograph of the effect of coma appears in Kingslake (37) and is reproduced in Figure 25.35.

(36) loc. cit., (26) 48, Plate II; also, Thesis, Groningen (1948)
(37) loc. cit., (28) 84, Plate IV

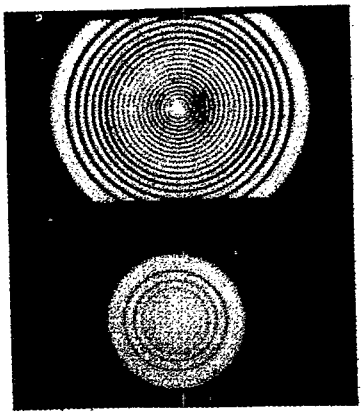

(a) Images in presence of primary spherical aberration of amount 16λ, at marginal focus and at circle of least confusion.

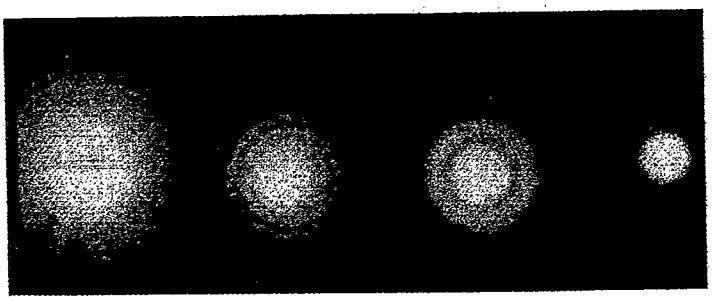

17.5λ 8.4λ 3.72λ 1.4λ

(b) Images in plane of paraxial focus, in presence of primary spherical aberration.

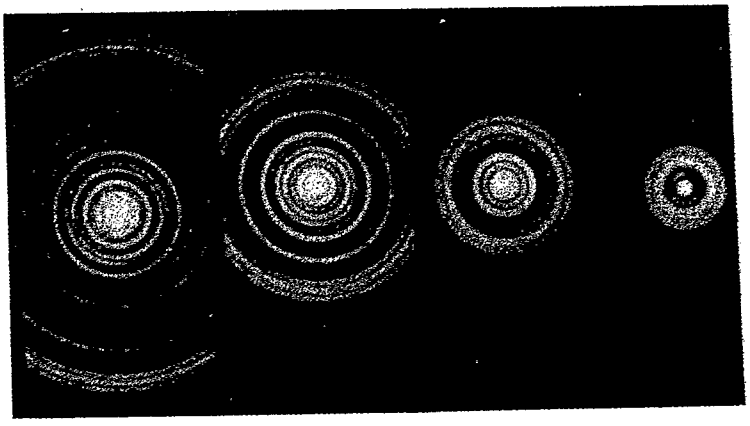

17.5λ 8.4λ 3.72λ 1.4λ

(c) Images in plane of least confusion, in presence of primary spherical aberration
scale three times that of (b).

Figure 25.34-Star images showing various amounts of primary spherical aberration.
(From Linfoot's, Recent Advances in Optics, Oxford Univ. Press, 1955)

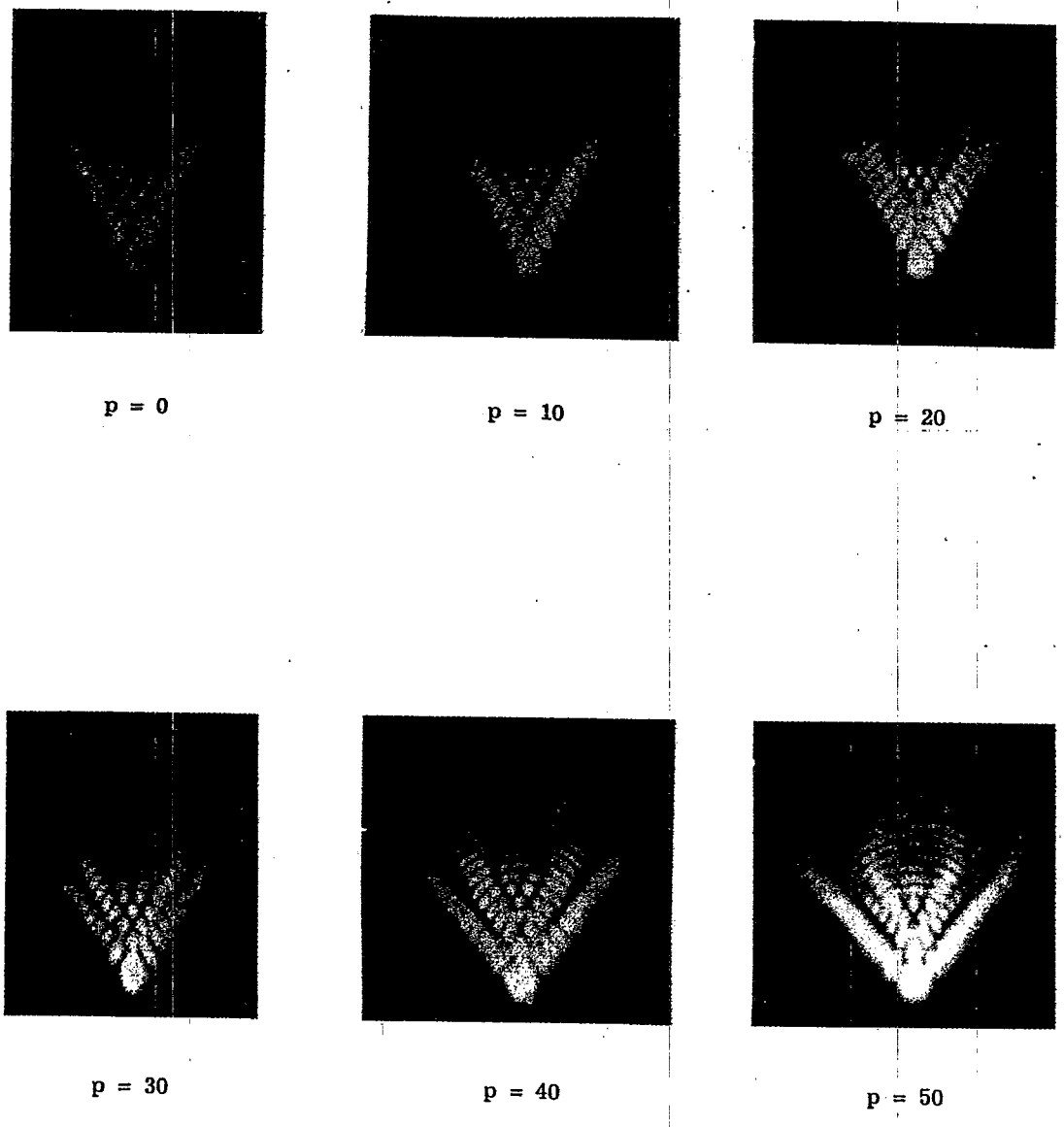

Primary coma - ϕ is $2\lambda (r^3 - 2/3\, r) \cos x$ at focal settings corresponding approximately to the given values of p.

Figure 25.35-Star images exhibiting coma.
(From Linfoot's, Recent Advances in Optics, Oxford Univ. Press, 1955)